December 2014

An Optogenetic Brain-machine Interface for Spatiotemporal Neuromodulation

Ryan Andrew Baumgartner
University of Wisconsin-Milwaukee

AN OPTOGENETIC BRAIN-MACHINE INTERFACE FOR SPATIOTEMPORAL

NEUROMODULATION

by

Ryan Baumgartner

A Thesis Submitted in

Partial Fulfillment of the

Requirements for the Degree of

Master of Science

in Engineering

at

The University of Wisconsin-Milwaukee

December 2014

ABSTRACT

AN OPTOGENETIC BRAIN-MACHINE INTERFACE FOR SPATIOTEMPORAL
NEUROMODULATION

by

Ryan Baumgartner

The University of Wisconsin-Milwaukee, 2014
Under the Supervision of Professor Ramin Pashaie

Direct neural stimulation has recently become a standard therapy for neurological disorders such as Parkinson's Disease, Essential Tremors, and Dystonia. Currently, deep brain electro-stimulation and neuro-pharmaceutical treatments are the dominant therapeutic options available to the public. As our understanding of brain function and neurological diseases improves, we are able to develop more advanced neuromodulation techniques. These methods could become viable treatment solutions for treating brain dysfunction. Optogenetics, first introduced by a research team led by Karl Deisseroth at Stanford University, has proved to be a versatile technique with remarkable potential to be used in treatments for brain disorders, dysfunction, and injuries. Optogenetics makes use of light-gated ion channels and pumps, originally derived from certain types of algae or bacteria, to bi-directionally modulate the activity of neurons in mammals. By adopting new advances in the field of optics and photonics, including high-speed high-resolution spatial light modulators, solid-state lasers, and ultra-low noise photodetectors, we can build sophisticated devices which allow precise and resolute optical patterning in both the spatial and temporal domains.

In this thesis, I present an optogenetic brain-machine interface that offers high spatiotemporal neuromodulation functionality. The incorporation of imaging and sensing devices of neural activity into the system allowed us to run multiple independent experiments. These optogenetic experiments include closed-loop modulation of multiple areas of tissue, investigating the causal relationship between neural activity and blood flow, and quantifying the relationship between neural activity and cell metabolism.

To understand light to brain tissue interaction in a rat brain, a device has been developed which allows one to extract the optical properties throughout the tissue. Utilizing this data, Monte Carlo software was used to predict light distribution within the brain. This has far reaching effects for the future use of optogenetics. Our approach will allow the investigator the ability to precisely understand how introduced light will be distributed within the rat brain where light-gated ion channels have been genetically expressed. This becomes noticeably important when attempting to determine which areas of the brain tissue will and won't be modulated by the introduced light.

Due to the many advantages optogenetics inherently provides, it is a rising prospect for novel neuromodulation therapies. With continued research and development of devices, we could create new therapies for disabilities that arise from dysfunction of the human brain.

TABLE OF CONTENTS

LIST OF FIGURES

see instances where the system is underdamped (0 s to ~250 s), overdamped (~250 s to ~350 s), and critically damped (~350 s to ~450 s). Figure adapted from [64]

Figure 23 – Visualization of a complex spatio-temporal closed-loop neuromodulation experiment. The upper left image shows the location of the photostimulus (the black square) and the photostimulus' related electrode number. The bottom row, which consists of three images, is the temporal sequence of applied photostimulus projection locations. The sequence of masks applied is as follows, projection mask #1 is available for projections for 100 ms, then projection mask #2 is available for projections for 100 ms, then projection mask #3 is available for projections for 100 ms, followed by a period of 700 ms when no projection mask is available for projection. This sequence is repeated for hundreds of seconds, data of which is displayed in the top right image. The top right image shows the measaured micro-ECoG values (in green) of all four electrodes involved in the closed-loop experiment, the activity set-point (in blue) for each of the four electrodes, and the photostimulus duration (in red), all through time which is the horizontal axis of the graphs. From this data, we can see that our spatio-temporal BMI has the ability to control multiple points which follow independent set-points over time. Figure adapted from [64]

Figure 24 – (Top Image) An image visualization of the 4 point closed-loop BMI experiment. This image consists of an intensity color (black equals little to no activity while white equals most increased activity) for all 157 sequences of the experiment. The electrodes which correspond to a given photostimulus are identified by the red rectangles and the square # located to the right of the image. The middle image is a visualization of the projection sequences. The bottom diagram is a block diagram of the electrode signal filtering and processing.

Figure 25 – The "artificial connection" experiment. This experiment is an experiment which was run to grasp the feasibility of bypassing nonfunctioning tissue within the cortex. In this experiment, we used a feedback system where the electrode measurements controlled the projection durations of photostimulus. The overall process is as follows: Site 1 is programmed to follow the set-point and site 2 is programmed to follow the electrical activity measurements from the electrode located at site 1 thereby allowing the activity signal from site 1 to be transferred to site 2 without these two locations being previously associated with each other. (b) It can be observed that the activity of site 1 follows the set-point, while site 2 slightly lags the activity of location 1 or location 1 follows the electrode measurements from location 2. This figure is adapted from [64]

Chapter I.   Introduction

1. Why invest in brain research?

The human brain is an extremely complex organ. The brain consists of approximately 100 billion neurons, and each of these neurons can have thousands of connections [1]. Attempting to understand brain function and connections are daunting tasks. Scientists' efforts could potentially yield invaluable information, which may impact our lives greatly. It seems that a large collaboration of highly dedicated scientists is the only feasible solution to understanding how this biological computer functions. In 2012, both the United States [2] and European Union [3] announced programs investing large amounts of funding towards understanding the brain function, connections, processing, and computational brain algorithms. These initiatives were announced independently; however, due to the complexity of the human brain, most likely these programs will become interdependent.

These initiatives are designed around the successful "Human Genome Project" [4] which not only completed the project goals but exceeded the expectations and had many

unforeseeable benefits. Financially, the economic impact was substantial. For every \$1 the US government invested the program returned \$141 [5]. The initiative accelerated our understanding of Genomics and it also allowed for developments related to bio-informatics, and aided in research across many fields in medicine and biology.

With 1 billion people affected by neurological diseases worldwide [6] investing in brain research seems imperative. Not only will investing in brain research help people suffering from neurological disorders, but it will open new doors for creating complex processing algorithms, intelligent machines, or inventing new architectures for complex parallel processing units. The brain is a parallel, non-linear processing organ capable of cognition. Understanding how our brain is able to understand our surrounding environment will benefit humanity greatly, possibly with greater impact compared with the human genome project.

2. Why develop Brain-Machine Interfacing devices?

The relatively recent computer boom has brought about new opportunities which aid in scientist's attempts to understand the human brain. Today, we have a better understanding of computation and processing than in the past. Using the innovations of computers and programming we have developed algorithmic models of neural networks, neural circuits, and brain function which have helped in our quest to understand the brain. Even with these algorithmic models, scientists still lack a fundamental understanding of human brain function. This disconnection inhibits our ability to cure or treat brain disorders and dysfunctions, directly investigate biological networks and circuits in-vivo and in-vitro, or to interface directly with our powerful information processing organ which is responsible for our well-being.

Using technology and our understanding of the brain, scientists are developing tools that are used to understand, communicate, and aid our brains. These brain-machine interface devices, which interface or communicate with the brain, have opened many new research opportunities and medical treatments that were extremely challenging if not impossible before.

3. Biological Inspired Sciences and Technologies Lab

Here at BIST labs, we devote our time developing tools which help us understand the brain and other biological processes as well as understanding the engineering principles adapted for realization of these tools. BIST lab employs the new technique of Optogenetics, explained later in this thesis, with a goal of furthering our understanding of neural circuitry and brain function. BIST lab's collaborators are experts in imaging, neuroprosthetics, and neuroscience and through our collaborations we create devices that potentially aid in brain research.

Chapter II.   Background

1. Neural Function

The brain is a collection of neurons (electrochemical non-linear biological processing cells), which when combined in complex networks with coded data, form the ability to understand their surroundings and adapt to win the evolutionary game of life. This is a very short yet complex description of the brain. We should start our journey by understanding how a single neuron functions.

In order to understand the most complex processes of the brain we must first understand the most fundamental discoveries that explain how a neuron functions. Ions, ion channels and pumps, and the membrane potential are all involved in neurons function. We should understand these elements to construct our understanding of neuron function.

Ions, ion channels and pumps, the cell membrane, the membrane potential, and how these elements work together to create the non-linear function of a neuron are an important part of understanding how the brain processes information. Inside and outside neurons there is a fluid that consists of many positively and negatively charged ions. In

this thesis we will think of ions as point charges, points in space of some positive or negative integer value charge. The difference of the net charge of ions inside the cell compared to outside of the cell is called the membrane potential. There are many pathways or gates located within the cell membrane for these charged ions to enter and leave a neuron. We call these pathways ion channels and ion pumps.

A. Ion Channels and Pumps

Ion channels are regulated by different mechanisms within the human brain. Naturally occurring regulators called neurotransmitters are able to open and close transmitter-gated ion channels by binding to neuroreceptors. Alternatively, channels can be opened or closed by voltage dependent mechanisms. These voltage dependent mechanisms are triggered by specific cell membrane threshold voltages. Certain threshold voltages are reached by the concentrated amounts of ions inside or outside the cell. This alters the cells membrane potential and triggers the opening or closing of the voltage gated ion channel. Transmitter-gated ion channels and pumps are generally involved in transferring a signal from a pre-synaptic neuron to a post-synaptic neuron or the transfer of signals between neurons. Voltage gated channels are responsible for the transfer of a signal within a neuron and triggering the release of neurotransmitters at the axon terminals.

B. Membrane potential

In order to better understand the function of a membrane potential, we imagine that there are three states in which the membrane potential may exist: a resting state, a firing state, and a restoring state. Refer to Figure 1 for a visual representation of these states with respect to a neuron's membrane potential.

C. Resting state

The resting state is the condition in which the ion concentration inside compared to outside the cell has reached equilibrium. At this point, the neuron is ready to receive input stimulation from other neurons. These connecting neurons either help to depolarize (raise the membrane potential) or hyperpolarize (lower the membrane potential) by interacting with the transmitter-gated ion channels located in the neuron's synaptic sites. The dendrites of a neuron may be connected to thousands of neighboring neurons. These neighboring neurons have a collective effect on the neuron's membrane potential. Neighboring cells can either help to depolarize the cell membrane, bringing the cell closer to the threshold voltage, or can help to hyperpolarize the cell membrane, keeping the cell membrane potential lower than the threshold voltage. As the membrane potential rises due to neighboring cell inputs, it will eventually reach a threshold voltage required to open the voltage gated ion channels.

D. Action state

When the membrane potential reaches the threshold voltage, the voltage gated sodium ion channels open allowing a large influx of sodium ions through the cell membrane. After a short period, the slower potassium ions start to open causing an outflux of potassium ions. The resulting spike in the membrane potential is called an action potential. The duration of an action potential is about 1ms. This action potential initiates at axonal hillock and propagates along the axon out to the axon terminals. At this point, synapses, located at the ends of the axon terminals, release neurotransmitters in order to pass this signal to its neighboring neurons.
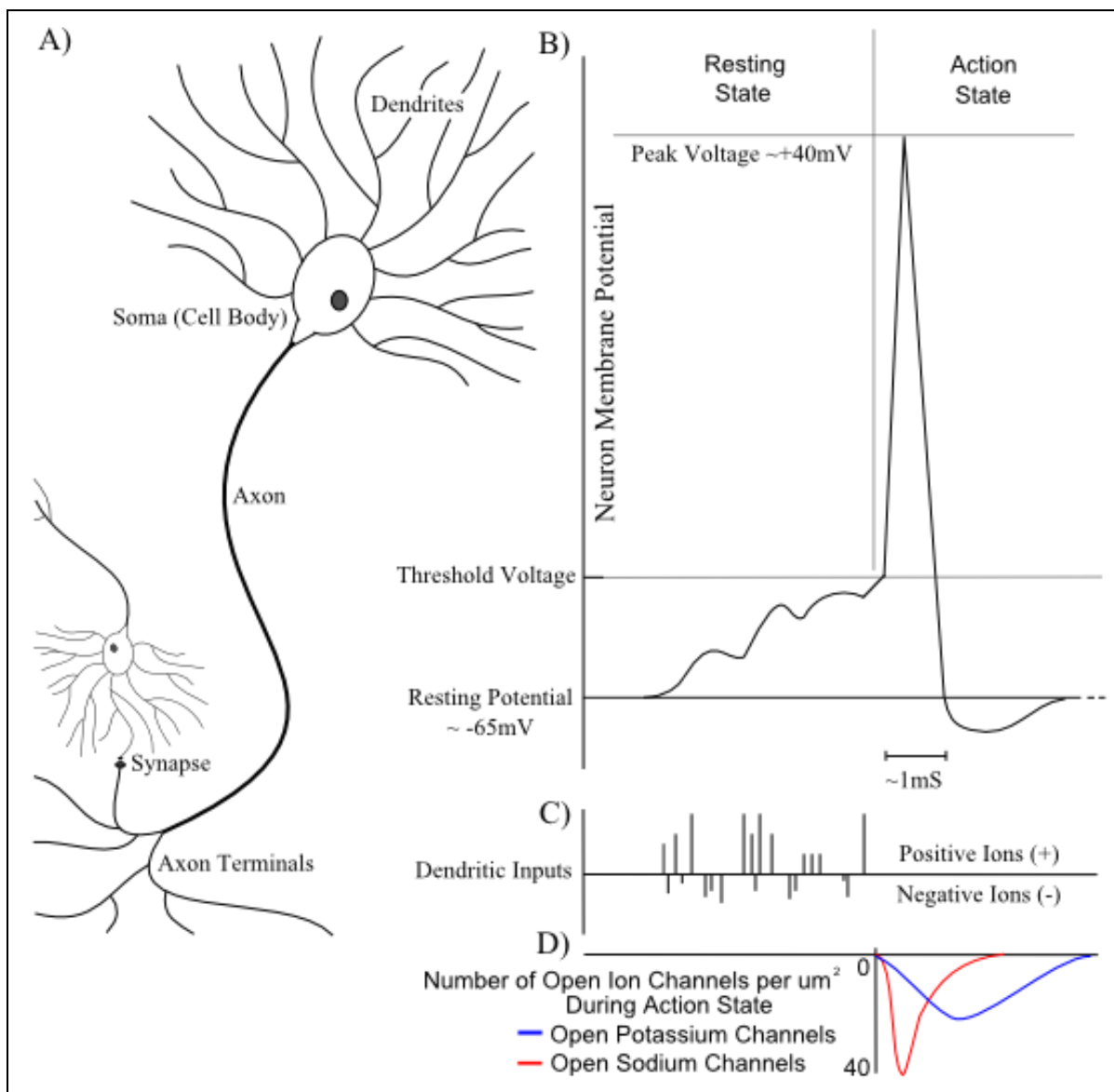
Figure 1 - A) Image of neuron anatomy. Dendrites receive inputs from connected neurons, the axon is a pathway for a neural signal to move from the soma to the axon terminals, the axon terminals and synapses are where signal transfer between neurons takes place. B) This is a visualization of the membrane potential during the Resting State and the Action State. C) Dendritic inputs are the source of inter-neuron communication. The charges of ions entering a neuron as dendritic inputs are cumulative. D) Dynamics of the voltage gated ion channels, potassium and Sodium. As the membrane potential reaches a threshold voltage, voltage gated ion channels open, causing a spike in the neuron's membrane potential called an action potential. The opening dynamics of these ion channels are the main source of the action potentials distinct shape. Sodium channels open fast causing an influx of positive ions. Potassium channels open and close slower causing outflux of positive ions. When combining the two channel dynamics, the net change in ions creates the action potential. Parts of figure adapted from [60] and [61]

Directly after this voltage spike, there is a period of time when the voltage gated

ions are closing and the membrane potential is being restored to the neuron's resting

potential (about -65mV). After the neuron returns to its resting potential, the resting state of a neuron's membrane potential begins to have an effect on the membrane potential.

E. Neurotransmitters and communication between neurons

A post-synaptic neuron is a neuron that has formed a connection through its cell body, dendrite, or axon with a pre-synaptic neuron. Neurotransmitters are released from the synapse of a pre-synaptic neuron, after an action potential, into the synaptic cleft where they are free to bind to neuroreceptors located on the post-synaptic neuron. Each type of neurotransmitters bind only to specific neuroreceptors. As these neurotransmitters bind with their respective neuroreceptors, the state of the transmitter-gated ion channel changes and directly affects the ion concentrations within the post-synaptic neuron. This change impacts the neuron's membrane potential, and thus the neuron's activity.

Neurons can be excitory neurons or inhibitory neurons depending on the types of neurotransmitters they produce. Excitory neurons, when transferring a signal, release neurotransmitters that create a flux of ions which have a depolarizing effect on the post-synaptic neuron. This flux of ions raises the membrane potential, bringing it closer to threshold voltage required for an action potential. Inhibitory neurons, when chemically transferring a signal, release neurotransmitters that create a flux of ions which have a hyperpolarizing effect on the post-synaptic neuron. This flux of ions reduces the membrane potential and keeps it further away from the threshold voltage required for the generation of an action potential. Both of these neuron types can be part of large groups of interconnected neurons called neural networks.

2. Neural Networking

Networks of neurons are self-organizing connections between many neurons which, when organized in a particular way, create a data processing apparatus. These networks are presented with an input signal that, as it propagates through the network, is filtered or coded. The connections in a network of neurons may change over time; this ability to change over time is called neural plasticity. These changes can occur because of environmental factors, injuries, change in lifestyle, etc. Network function can range from simple edge detection within the visual cortex to complex face recognition and motor functions.

Neural networks start their processing using sensory inputs from our sensory organs: visual, somatosensory, auditory, gustatory, and olfactory. Each of these sensory systems has cells or mechanisms that quantify their specific sense. The visual system uses light sensitive cells called photoreceptors, which are present as either rods or cones, to quantify photons into neural signals. The auditory mechanism is a collective structure of separated air chambers, tiny bones and membranes which are able to separate and quantify air pressure waves into their frequency components. The quantification of these sensory inputs now becomes inputs to neural networks.

Each sensory input travels through distinct pathways in the brain. As the signal propagates through these pathways the input is processed. This processing extracts information from the inputs, which our brain uses to classify our surrounding world. These information-processing networks are complex combinations of cells, which have a remarkable ability to collectively understand our surroundings through our sensory inputs.

In order to understand complex networks, we must first understand the simple microcircuits that occur within the brain. These microcircuits are the interactions between different types of neurons (for example inhibitory and excitory) and different connections between them. These distinct microcircuits are considered the building blocks of large networks within the brain as they combine and expand to create complex networks with specific functions. These complex networks are what enable us to extract and remember information from our surrounding environment in order to make decisions. Some possible building block microcircuits, or micronetwork motifs are described in Figure 2.

Expanding upon and combining these simple microcircuits allow for the development of highly connected and complex networks with specific function. One example of the function of these complex networks is edge detection which is used extensively in our visual system.

3. Temporal Firing Rates and Frequency Coding

Frequency coding or rate coding refers to the phenomenon of information being represented within the frequency of neural spikes. An experiment conducted by E. D. Adrian, where he stimulated the sterno-cutaneus muscle in a medium sized frog, to demonstrate that the frequency of nerve impulses increased as the force on the muscle increased [7]. 0.5 grams resulted in a frequency of 35 impulses per second directly after loading and after 10 seconds of loading it reduced to 15 impulses per second. 1 gram resulted in 66 impulses per second directly after loading and after 10 seconds of loading it reduced to 37.5 impulses per second. How information is coded within the brain is still an active area of research but it is important for us to remember that information from our

surroundings are coded into signals which become the inputs for the neural networks within our brains.

Neural Network Building Blocks - Possible Microcircuits	
Type of Connections	Description
Feedforward Excitation	Presynaptic excitory neuron relays information to it's connected postsynaptic excitory neuron. Long chains of feedforward connections are able to propagate a signal through the nervous system.
Feedforward Inhibition	The combination of an excitory neuron stimulating an inhibitory neuron which inturn inhibits the next neuron. This type of combination will limit or inhibit activity of the third neuron.
Convergence/Divergence	Convergence is the process of one neuron receiving many inputs from a number of neurons. These inputs can be both excitory as well as inhibitory. Divergence is the process of one neuron to communicate with many other neurons.
Lateral Inhibition	An excitory neuron excites inhibitory neurons which will inhibit neighbors of the excitory neuron.
Feedback Inhibition/Excitation	Feedback circuits allow a stimulated neuron to either inhibit or stimulate a neuron which provides the neuron inputs.
Recurrent Inhibition/Excitation	Recurrent means turning back in a direction opposite to a former course. In the neural circuit cases, these combinations of connections ultimately end up leading back to the original neuron. These can be both inhibitory or excitory. The excitory neuron can directly stimulate itself, this case is called an autapse.

Key: Inhibitory Neuron   Excitory Neuron   Could be either Excitory or Inhibitory

Figure 2 - Description of possible microcircuits made by combining Inhibitory, excitory, and different types of connections between them. This figure is adapted from figure 6 in citation [62]

4. Neurons and Oxygen

Oxygen is crucial to the health of brain cells and these cells receive oxygen contained in blood that comes from our lungs. Oxygenated blood is so important to functioning brains that our bodies will redirect blood flow to the brain in a case of lowered blood oxygen levels. The brain requires approximately 3.3 mL of oxygen per 100 g of brain tissue per minute [8]. This is roughly 17.82% of our total oxygen consumption (Average brain weight *Oxygen consumption per 100 grams brain mass). This means that approximately 2.18% of our body weight (Average brain weight/Average human body weight) consumes 17.82% of our blood oxygen.

A widely accepted relationship between neural activity and oxygen consumption is that as neural activity increases, oxygen consumption also increases [9]. This relationship has become extremely important in brain research due to our ability to monitor blood oxygenation easier then monitoring brain activity directly. Functional magnetic resonance imaging (fMRI) is a widely used device for monitoring blood oxygenation by measuring the blood oxygenation level dependent (BOLD) signal.

5. Neurons and Metabolism

The brain needs energy to function! More specifically, the brain needs glucose to power its function. Glucose can be incorporated into lipids, proteins, glycogen, and is also the precursor of certain neurotransmitters. The brain accounts for 25% of our body's glucose utilization [10]. Just as with oxygen, scientists have formed a connection between neural metabolism and neural activity. A widely accepted relationship between neural activity and metabolism is that as neural activity increases, metabolism in turn increase.

6. Introduction to Neural Modulation

An important technique that can be used to investigate neural circuitry is neuromodulation. We consider neuromodulation as a technique used to control or modulate the activity of neurons using an externally controlled source. Today, scientists have developed many different types of neuromodulation techniques. These techniques use our understanding of neuron function to cause an increase or decrease in neuron activity. Having the ability to precisely control the activity of neurons and neural tissue allows us the opportunity to correct dysfunction within neural networks in our brains [11]. Neuromodulation allows scientists to study the functions of specific areas of neural tissue. For example, by stimulating different areas of the motor cortex, scientists have developed detailed relational maps between motor (movement) actions and areas of neural tissue in the motor cortex [12]. Our understanding of brain function seems reliant on our ability to modulate neural tissue. Ideally, a neuromodulation technique would have a spatial resolution below the size of a neural cell allowing for spatial targeting in the cellular range, and a temporal range of stimulation in the range of a single action potential.

A. Electrical Modulation Technique

One well-known and widely used technique for modulation of neural tissue is electrical stimulation. Scientists use our understanding of electric charge to interact with neural membrane potentials. By introducing an electrode of negative charge in an area of neural tissue, researchers can stimulate neurons in the surrounding area. Researchers have created many different arrays of electrodes with varying size, number of electrodes, penetrating and surface mount electrodes, compositions, and electrical designs. While

this technique has been used nearly exclusively throughout history for neural experiments and treatments for brain disorders, there are many limitations of electrode arrays.

Electric stimulation can only directly stimulate areas of neural tissue. In order to inhibit areas of neural tissue, researchers must indirectly cause inhibition by stimulating inhibitory neurons. This seems problematic for neural probing as our knowledge of specific neural connections is still vastly unknown. Implanting electrodes into neural tissue also poses problems such as damage to tissue, infections, and even our immune systems can hinder electrode effectiveness. The sizes of electrode arrays are limited by manufacturing processes and also by the amount of damage they cause to the neural tissue when implanted. Another issue is that electrode arrays have low spatial resolution compared to the size of neurons.

B. Optogenetics – An optical Neural Modulation Technique

In 2005, a new technique developed for neural modulation, Optogenetics [13], was introduced by the Deisseroth lab at Stanford University. Using genetic techniques, Karl Deisseroth and his lab members were able to successfully express DNA, originally found in algae, in mammalian neurons. The expressed DNA includes the genetic code or instructions for a cell to produce specific opsins. These opsins are light sensitive receptors which were used by the algae to sense their source of energy. In neurons, these opsins are used to modulate the activity of neurons with light. I will present two specific opsins in this thesis, a light-gated cation channel, Channelrhodopsin-2 (ChR2), and a light-driven chloride pumping halorhodopsin (NpHR). ChR2, when exposed to light of approximately 445nm wavelength (Refer to Figure 3 for a more detailed spectrum of stimulation wavelengths for ChR2), allows Na^+ and Ca^+ into the cell which raises or

depolarizes the membrane potential and leads to an action potential. NpHR, when exposed to light of approximately 570nm wavelength, pumps chloride ions into the cell which hyperpolarizes the membrane potential thus inhibiting the neuron from firing (Refer to Figure 3 for a more detailed spectrum of stimulation wavelengths for NpHR).

ChR2 and NpHR allow for stimulation and inhibition of genetically targeted neural populations on the millisecond timescale [14]. In Figure 3(C), you find an experimental demonstration of both ChR2 (neural stimulation) and NpHR (neural

Figure 3 - A) Left image shows channelrhodopsin-2 (ChR2), Right image shows halorhodopsin (NpHR). ChR2 allows Na$^+$ into the cell when activated by blue light. NpHR pumps Cl$^-$ into the cell when activated by yellow light. B) Spectral activation of ChR2 and NpHR. Given the maximum locations for both are located approximately 100nm from eachother, it is possible to simultaneously stimulate using ChR2 while inhibit using NpHR C) Experimental demonstration of both stimulation using ChR2 and inhibition using NpHR. This figure is directly adapted from "Circuit-breakers: optical technologies for probing neural signals and systems." [63]

inhibition). In Figure 3, we notice that NpHR is able to suppress neural action potentials even when cells are stimulated with ChR2 and blue light. The development of novel optical devices allows for large scale neural network probing with high spatial and temporal resolution. The optogenetic technique allows for cell-type specific targeting [15] by using appropriate promoters. Another unique benefit of optogenetics is having the ability to bi-directionally control the cellular activity of neurons directly. By having the ability to express both light-gated cation channels and light-gated anion pumps into neurons simultaneously, one has the ability to either increase neural activity or suppress neural activity [14][16]. Another benefit of using light as the source for activating the ion channels lies within our ability to manipulate light to form images or patterns which are both temporally and spatially dependent. In this thesis, I will introduce such a device for patterning stimulating light with megapixel resolution and the ability to target specific areas contained within the field of view.

7. **Introduction to Neural Monitoring**

Just as important to neuromodulation for investigating neural circuitry is having the ability to monitor neural activity or something that indicates neural activity. Current techniques and devices used in monitoring neural activity vary widely in both temporal resolution as well as spatial resolution. Not only do these techniques vary in resolution but they also vary in what specifically they monitor. These monitoring devices measure oxygen in blood, the metabolism of cells and tissue, local field potentials, actual membrane potential of a neuron, or even the concentrations of calcium inside of a neuron. Through years of research and investigation of neural function, scientists have developed

and/or are still developing relationships between these neural activity indicators and neural activity.

The functional Magnetic Resonance Imaging (fMRI) technique uses a relation between a blood oxygen-level dependent (BOLD) signal and neural activity. Functional MRI has become a monitoring device which dominates brain research. Functional MRI has acceptable spatial resolution with the ability to monitor the whole human brain. Functional MRI has a relatively low temporal resolution mainly due to the nature of blood flow within the brain and how blood flow changes in response to neural activity. Positron Emission Tomography (PET) monitors the metabolism of neural tissue and uses a relationship established between metabolism and neural activity. As neurons are more active, the energy usage increases thus metabolism increases. PET machines use this intertwined relationship to image brain activity. Electroencephalography (EEG) and Electrocorticography (ECoG) both measure local field potentials (LFP) or collections of neural activity. EEG measures LFPs from the surface of the scalp while ECoG arrays are implanted directly onto the surface of the brain from where they measure LFPs originating in the cerebral cortex. Spatial resolution of ECoG is better than EEG's resolution because are placed closer to the brain tissue. The membrane potential of a neuron can be measured using a technique called patch clamping. The patch clamp technique measures the membrane potential by placing one electrode inside the cell while having another electrode just outside the cell. The difference between the electric potential recorded by these electrodes is the membrane potential. Fluorescence imaging allows for measuring changes in metabolism, blood flow, and even concentrations of specific ions within neurons. This type of imaging is versatile and has been used for

many applications. Pairing fluorescence imaging with neural modulation techniques offers additional advantages such as targeting the activity of specific cell types.

8. Introduction to Brain-Machine Interfacing

A brain-machine interface (BMI) is a device which interfaces directly with brain. There are three possible interactions that can be implemented via BMI application. These interactions are monitoring the activity of neural tissue and perform some sort of external action, taking input from a person's surroundings and modulate neural activity according to this external input (sometimes called a neuroprosthetic device), and modulating the activity of one area of neural tissue according to the monitored activity of another area of the tissue. The last type of interaction for a BMI can be realized in the form of a closed-loop BMI device because its interactions are solely within the brain. A BMI device, theoretically, can use any type of device which monitors or modulates neural activity. We decided to use Optogenetics for neural modulation and Fluorescence Imaging and ECoG recording for monitoring when designing our optogenetic brain-machine interface. During experiments, with our collaborators at the University of Wisconsin-Madison, we integrated a transparent ECoG into the experimental set-up [17].

9. Neural disorders and Current Treatments

The goal of neuromodulation and Brain-Machine interface research is the ultimate realization of real world treatments and therapies for neurological disorders, diseases, and injuries using any of the various neuromodulation techniques. In order for neuromodulation to be described as a therapy, defined by K. M. Alo and J. Holsheimer, it must be an ongoing, dynamic intervention that affects specific neural networks and its clinical effect is continuously controllable by varying stimulation parameters [18].

Neuromodulation techniques, therefore, can include any method to alter the activity of neurons in a controlled manner.

One of the most developed techniques is Deep Brain Stimulation (DBS) utilizing electrodes as the method for altering neural activity. As early as 1969, chronic DBS of the thalamus, straitium, and pallidium has been used to treat movement disorders [19]. As research in DBS has matured, there have been therapies for essential tremors [20] and Parkinson's Disease [21]. Current neuromodulation therapies for epilepsy include vagus nerve stimulation, and DBS [22]. DBS has also provided therapies for neurobehavioral disorders such as Obsessive Compulsive Disorder and treatment-resistant depression [22]. DBS has had success in relieving chronic pain and neuropathic pain syndromes [22]. DBS is also being applied as therapies for Tourette's Syndrome [23,24], obesity [25], dementias [26][27], addictions [28], tinnitus [29], and anorexia [30]. Another type of modulation currently used to offer treatments for the management of spasticity and pain is chemical. Chemical modulation usually consists of devices which allow chemical compounds to pass through the blood brain barrier [22].

While these types of neuromodulation have been successful for many types of neurological disorders, they lack the ability to control where and which cell types they target to modulate activity. Having the ability to stimulate specific types of neurons using genetic targeting [15], directly inhibit neural populations [16], or precisely controlling the modulating mechanism, similar to what is described in this thesis, could create safer therapies for the already established therapies which use DBS, electrical, or chemical neuromodulation. Optogenetics, using gene therapy to introduce light-gated ion channels into neurons, has many of these advantages which could allow previously not-feasible

therapies to be realized. Introduced in 2005, optogenetics is still in the early stages of developement and has yet to be fully developed. One exciting prospect is using a spatial temporal light projection system to target cortical areas of the brain in order to supplement loss of sensory networks which have been disrupted by brain injuries such as those caused by stroke. The success of optogenetics will come from its natural advantages over current techniques. It seems unlikely that current companies who are leaders in neuromodulation device development would stop researching and furthering the already developed electrode technologies for therapies which utilize optogenetics. However, as long as the limitations of electrodes lags behind the potential for improved neuromodulation therapies using optogenetics, there will be a demand to realize the true potential of optogenetics.

Chapter III.   Optogenetic Brain-Machine Interface Design

1. Design Overview and Design Goals

The development of a device which has the ability to monitor neural activity and/or biological functions of tissue as well as simultaneously modulate, both inhibit and stimulate, neural tissue with a spatial resolution of a single neuron and a temporal resolution of an action potential will enable researchers a unique opportunity to investigate how the brain networks process information. Understanding how networks of neurons process, store, and recall information from our surrounding world appears to be an important aspect of brain research.

Using the newly established field of optogenetics, we now have the ability to directly stimulate and inhibit neurons using light. As discussed earlier, using ChR2 and blue light, we can open ion channels which allow positive sodium ions into the cell, and using NpHR and yellow light we can activate an ion pump which pumps negative chloride ions into the cell. Recalling that as a neuron's membrane potential becomes more positive it may reach a threshold voltage at which the cell has a large membrane potential spike caused by voltage gated ion channels. This large membrane potential spike passes the

signal along the neuron's axon and to the ends of the dendrites where the signal is chemically relayed to post synaptic neurons.

Not only does using optogenetics and light provide direct and precise control of neural tissue modulation, many optoelectronic devices have been developed over the years and are used to modulate light spatiotemporally. Using these spatiotemporal light modulating devices, we could imagine the possibility of being able to target specific neurons or groups of neurons which we would like to modulate. Having an ability to target groups of neurons opens the possibility of probing or applying inputs to targeted

Figure 4 – The future hardware design for our Brain-Machine Interface. Each section is discussed in depth in the next section. Some features displayed in this image are not available with the current implementation. See Figure 15 for the current progress of the device.
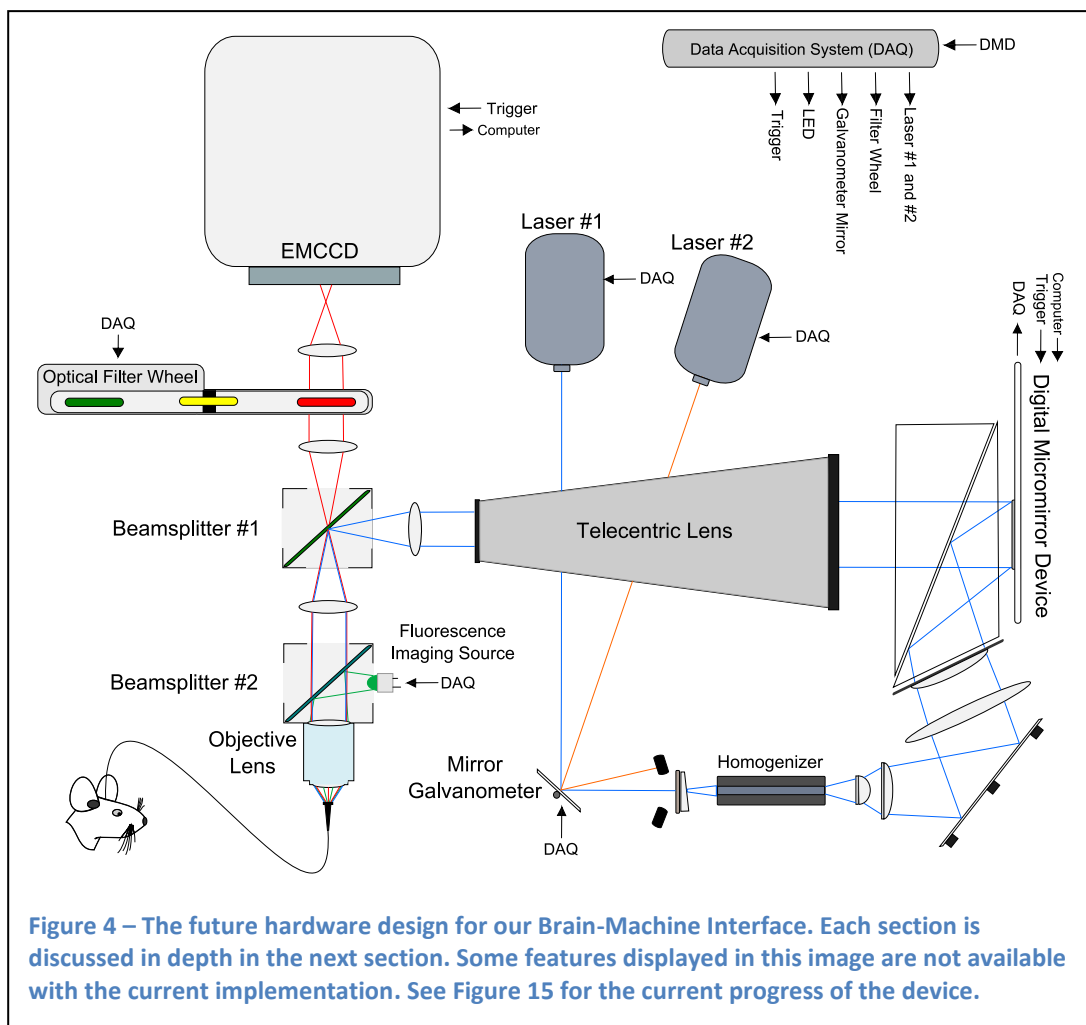
neurons while avoiding surrounding non-targeted neurons.

In order to probe neural circuitry, we must be able to record the activity of these neurons. Ideally, we would like to record the activity of all neurons simultaneously with a temporal resolution similar to that of an action potential. Many functional fluorescence molecules have been used to record neural activity [31]. Along with intrinsic fluorescence molecules, such as NADH (nicotinamide adenine dinucleotide) and FAD (flavin adenine dinucleotide), which are both involved in cell metabolism, there are genetically expressed fluorescence molecules which can provide information about the membrane potential, or can provide information about ion concentrations within a cell, such as calcium indicators. Among these fluorescence molecules, some have the ability to function on similar temporal scale as neural action potentials.

Along with using an imaging path to monitor neural activity, we can use our imaging device to make spatial geometrical relations between the location of samples which we are imaging and our projection path which is used to modulate the samples. These spatial relations make possible our ability to spatially target certain areas of the sample. Combining all of these functions: bi-directional neural modulation, monitoring neural activity, and targeting, into one device will enable the possibility of methodically investigating neural circuitry.

2. Device Development

A. Optogenetic Projection Path

A block diagram of the projection path of the device is illustrated in Figure 5. We implement a high powered blue (2 Watt, 445 nm) laser for our optogenetic stimulation. The laser beam is homogenized by an integrating rod and collimated by a telecentric

illumination lens mechanism before exposing the active area of a Digital Micromirror

Device (DMD) through a total internal reflection (TIR) prism. The TIR prism, which is

placed in front of the DMD, guides the beam of light to illuminate the DMD surface at an

angle of 24 degrees, see Figure 6 according to the specific design of micromirrors on the

DMD chip. This prism also separates the illuminating beam from the modulated reflected

beam.

The DMD (Model – DLP Discovery 4100 0.7 XGA) consists of a 1024 by 768

matrix of tiny mirrors (13.6 micrometer pitch) which are programmatically controlled to

reflect projection light into the lens or reflect the light away from the lens. Our DMD

Figure 5 - Projection path block diagram. Laser light originates from the laser. Propagates through the homogenizer and diffuser, and then enters the optical engine for the DMD device. The light is then spatially modulated and projected through a telecentric lens, beamsplitter #1, and finally the objective to the sample.
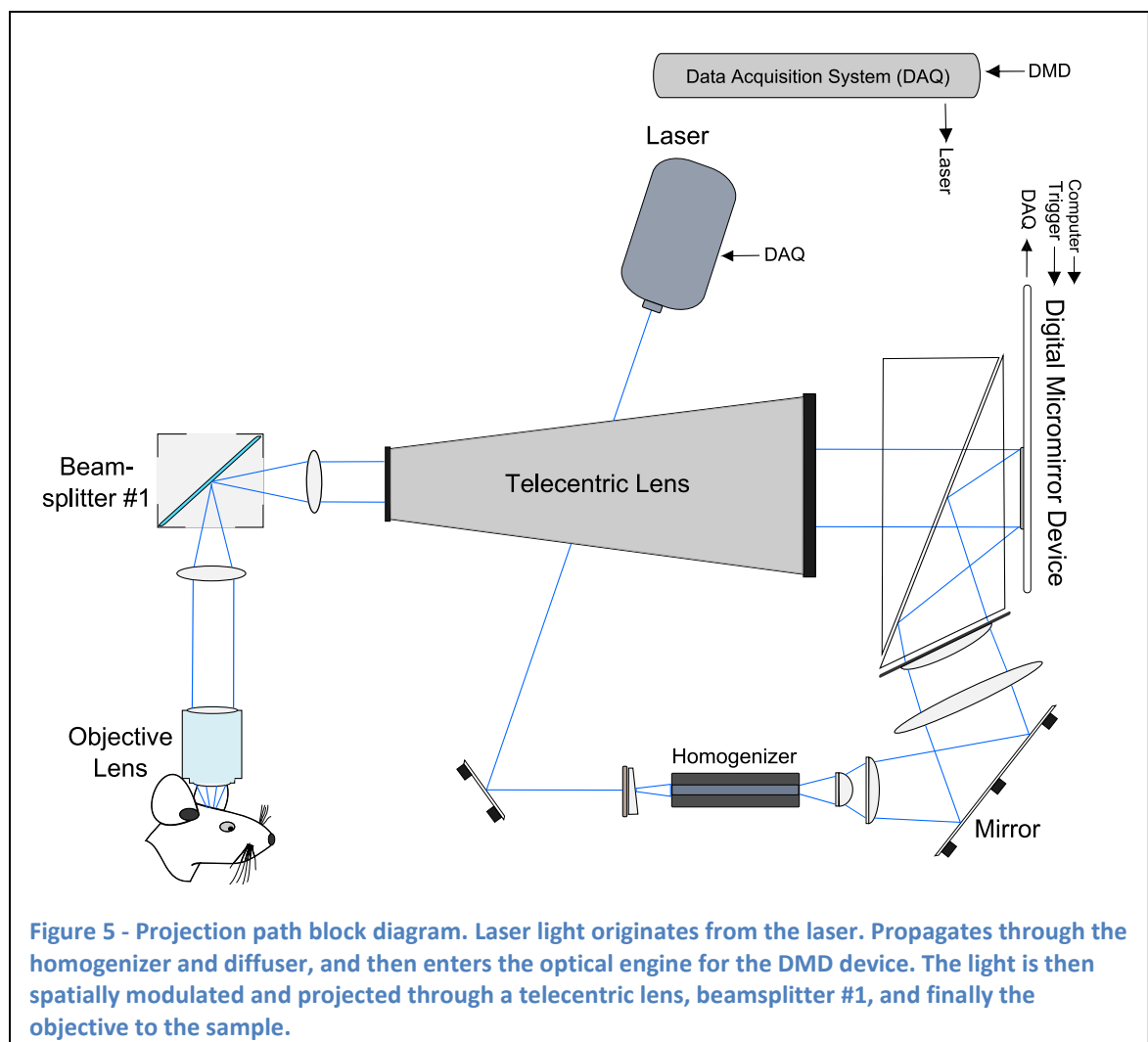
chip can display up to 32,552 binary frames a second or 290 8-bit grayscale images [32] [33]. This speed and high resolution allows us to display grayscale images on the same time scale of neural activity with megapixel resolution which should allow the device to simultaneously modulate a neuron's activity independently. For our experiments presented later, the DMD was used to create pulsed laser trains of spatial photostimulus patterns. Rather than modulating the power of the laser, we set it to full power and create the pulses by toggling the DMD, effectively creating a pulsed laser signal.

DMD systems require uniform angles of incidence across the entire modulation

Figure 6 - Digital micromirror functionality on DMD chip. Each one of the 768 by 1024 mirrors can be independently controlled to be either on or off. The flat energy state occurs when the DMD is not initialized. After initialization, the mirrors enter the off state.
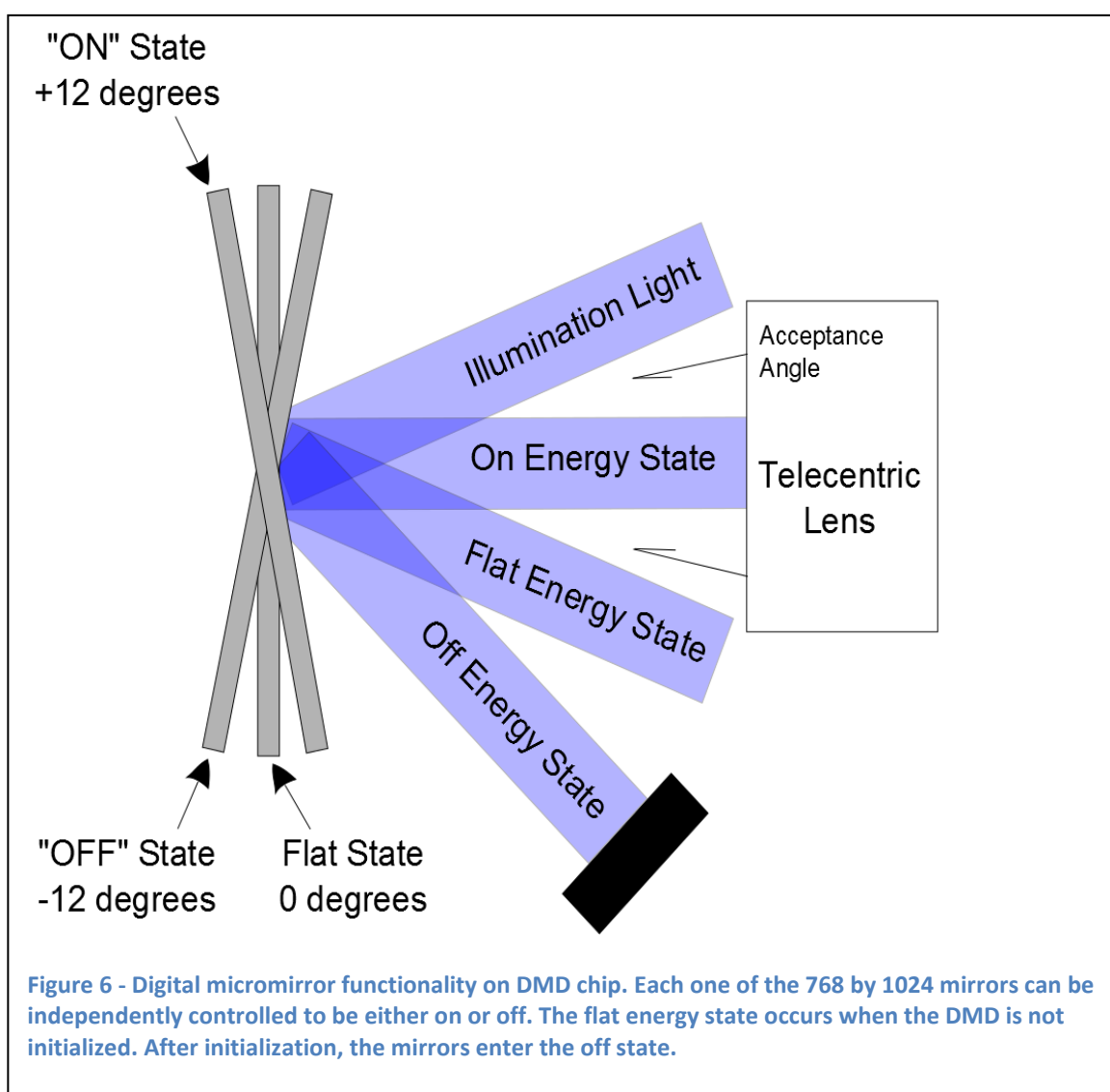
screen [32]. To provide this illumination, telecentric illumination architecture is introduced directly before the DMD. In telecentric systems, the optical pupil is at infinity. This means that the chief rays for each point in the illuminated image field are parallel and each DMD micromirror is illuminated with a cone of light incident at the same angle. The spatial light modulator which we integrate in our design, DLP4100 by Texas Instruments, uses a TIR prism to systematically separate the light from the telecentric illuminator and the light reflected by the DMD. All light rays incident on the TIR surfaces which are below a specific incidence angle, light from the telecentric illuminator, are reflected onto the DMD. The modulated beams are sent back to the TIR surface at angles such that they are now transmitted through the TIR prism and into the projection optical system.

In a projector, the illumination optical system, the modulator device, and the projection optical system (i.e., the projection lens) form a single complex optical system. Each of these three modules optically "interact" with each other and their respective designs must carefully adhere to specific interface requirements. When full performance is required, the projection lens should be designed specifically for use with a particular illumination optical architecture. In our system, we must take into account the illumination pupil position, the thickness of the TIR prism and the DMD mirrors, the size and resolution of the DMD, and the f/# of the illumination system.

The modulated beam, transmitted through the TIR prism from the DMD micromirror array, enters a telecentric lens. This telecentric lens ensures that only the rays reflecting directly perpendicular with the DMD face enter the system. This is important when trying to avoid areas of tissue with the photostimulus light. If light were

able to enter the telecentric lens at an incident angle of 24 degrees, the "off" mirror angle of the DMD, then stimulus light could possibly excite an optogenetic opsin in a non-targeted area. The projection optical system accepts these rays of light, transmits, and refracts them in such a way as to produce an image of the DMD mirror array surface onto a remote screen or at a suitable intermediate image plane to be captured by yet another optical system, an image combiner (Photometrics, DC2). The telecentric lens also scales down the image created by the DMD by a factor of 2 and projects the pattern on the entrance pupil of the image combiner or beamsplitter #1. The image combiner is an assembly of mirrors, lenses, and a replaceable dichroic or a beam splitter with two polarizers (shown in Figure 5 and Figure 15 as beamsplitter #1).

Beamsplitter #1 could be any component which has the ability to separate two separate sources of light. This component creates a junction between the optogenetic projection path and the fluorescence imaging path. Choosing this optical component depends solely on your experimental application.

The first consideration and most important consideration when choosing which optical component to use for beamsplitter #1 is the type of optogenetic opsin we intend to use during our experiments. Although many new opsins are being discovered, there is still a limited selection available and careful consideration should be made when choosing an opsin. Our focus when choosing an opsin, on an experimental design level, is the opsin's excitation wavelength and function. The excitation wavelength must be reflected to the sample when it comes in contact with optical component #1.

The second consideration when choosing beamsplitter #1 is the fluorescence emission wavelength which will be used for neural monitoring. Depending on the

biological process which you would like to investigate, there are many fluorophores or fluorescence molecules to consider. There are a wide variety of fluorophores available which allow monitoring from many different biological processes such as, vascular processes, metabolic processes, neural ion concentration, and cell voltage sensitive dyes, all of which can be chosen to fit into your experimental needs.

When looking at Figure 5, one can notice that the optogenetic stimulating light is reflected by beamsplitter #1 while, in Figure 8, the fluorescence imaging wavelength propagates from the sample through beamsplitter #1 onto the camera's sensor. One optical component which has this property is a dichroic mirror. One set of beamsplitter configurations for the projection wavelength, fluorescence emission wavelength, and beamsplitter #1 for the device is displayed in Figure 7. We see that our blue optogenetic stimulation light is reflected by beamsplitter #1 while our emission fluorophore wavelength is allowed to pass through the component to the camera.

Figure 7 - This figure illustrates an example of optical components adapted for our neurovascular coupling experiment. Beamsplitter #1, in figure 5, reflects the selected opsin's stimulating wavelength (~445nm) while it allows the fluorescence emission wavelength to transmit through toward the camera. Beamsplitter #2, in the same figure, allows for the introduction of the excitation wavelength for Rhodamine B isothiocyanate-dextran (Sigma, 70 kDa) while also allowing both the opsin stimulating wavelength and fluorescence emission wavelength passing through.

B. Fluorescence Imaging Path

Fluorescence imaging requires illuminating fluorescence molecules with an excitation wavelength. An excitation wavelength source provides the energy for the fluorescence molecule to emit light of a lower energy level. We introduce a beamsplitter, beamsplitter #2 in Figure 8, to deliver light of an appropriate fluorescence excitation wavelength into the system. This beamsplitter must allow the fluorescence signal and the optogenetic excitation wavelength to pass through while reflecting the fluorescence excitation light to the sample. We have used one excitation

Figure 8 - Fluorescence imaging path. The excitation light for Rhodamine B isothiocyanate-dextran (Sigma, 70 kDa) is introduced at beamsplitter #2. This propagates to the sample. The fluorescence emission light is captured through the objective. There is an optical filter directly in front of the camera to eliminate unwanted light from being imaged by the camera.

source for each of our experiments, discussed in detail later, that involve fluorescence, a wide-spectrum high-power light source filtered to a specific wavelength bandwidth and a high power ultra violet (UV) LED.

The wide-spectrum high-power source produces light which passes through one of four user specified optical filters. The optical path is controlled by a galvanometer mirror that directs the source light to a pair of parabolic mirrors and then injected into a

homogenizing light guide. Between these two mirrors, the light passes through a hot

mirror, to reduce the infrared power, before being filtered by the appropriate optical filter.

We use sputter-coated high-transmission fluorescence excitation filters which are capable

of withstanding the absorption of large amounts of optical power from being mounted

close to the high-power source.

As the fluorescence excitation light hits the sample, it causes the fluorescent

molecule to fluoresce emission light which corresponds to a biological process under

monitor. This emission fluorescence signal propagates from the sample through the

imaging path eventually becoming incident on an imaging sensor. As this signal

propagates through the imaging path it passes through a number of components: an

objective lens, beamsplitter #1 and beamsplitter #2, a collimating adaptor, and optical

emission filters.

To ensure the light measured by our imaging sensor is the only light from our

fluorescence emission signal, we place optical emission filters in the optical path. A high

speed filter wheel holds the emission filters in place between beamsplitter #1 and the

imaging sensor within a collimating emission adaptor.

The collimating adaptor is required for two reasons as demonstrated in Figure 9(a)

and (b). Anytime a flat piece of glass with a refractive index different from air is inserted

in a focusing beam, the beam no longer focuses at its original location; instead, the

location of the focal plane is shifted. The amount of shift depends on the thickness of the

filter as well as the index of refraction of the glass used to make the filter. The second

reason is the bandpass quality of the filter which decreases as the incident light's angle

changes from 0 degrees. The collimating emission adaptor creates an area of collimated

light which allows the addition of other optical devices, such as a filter wheel, without

sacrificing on the performance or introducing optical aberration, Figure 9(c).

Figure 9 - Light incident to color filters should be collimated to ensure that the imaging focal plane is not affected by the change in refractive index of the color filters. (a) shows the shift in the focal plane after a section of glass is introduced in to the system. (b) shows a complication which arises from this type of aberration. (c) shows a diagram of one solution to fix this issue which is to collimate the light before it passes through the glass section.

Many fluorescence molecules, such as NADH, have faint signals; therefore, to

improve our fluorescence detection capability, we have used an Electron Multiplying

Charge Coupled Device (EMCCD) as our fluorescence detector. We chose the

photometrics Evolve 512 EMCCD (photometrics, Tucson, AZ, USA) for its high

quantum efficiency and ease of integration into our system. The imaging sensor consists

of a 512 by 512 imaging array while each pixel is 16 by 16 micrometers. The imaging

sensor can detect light from 350nm to 900nm and at its maximum has a quantum

efficiency of >95% [34].

It is vital that the system, in particular the DMD and the EMCCD, be fully

synchronized. Any lack of synchronization could cause considerable fluctuation in

images captured by the EMCCD. This systematic error may be misinterpreted as

fluorescence changes produced by cellular activities. In order to synchronize all the

elements of this setup, we have implemented trigger coding throughout the BMI device.

Focusing of both the imaging path and projection path is achieved by a separate

lens mechanism, a microscope objective, which is mounted after beamsplitter #2. Our

imaging device is mounted on a three dimensional translation stage in order to center the imaged signal and fine tuning of the parfocality between the projection and imaging paths.

3. Device Realization

The implemented optogenetic Brain-Machine Interface has demonstrated spatial temporal modulation of neural tissue (we have only demonstrated neural stimulation using blue light and ChR2), monitoring neural activity using fluorescence, injected dyes (vascular response due to optogenetic stimulation) and intrinsic fluorescence (NADH and the metabolic response due to optogenetic stimulation), and automated targeting of areas
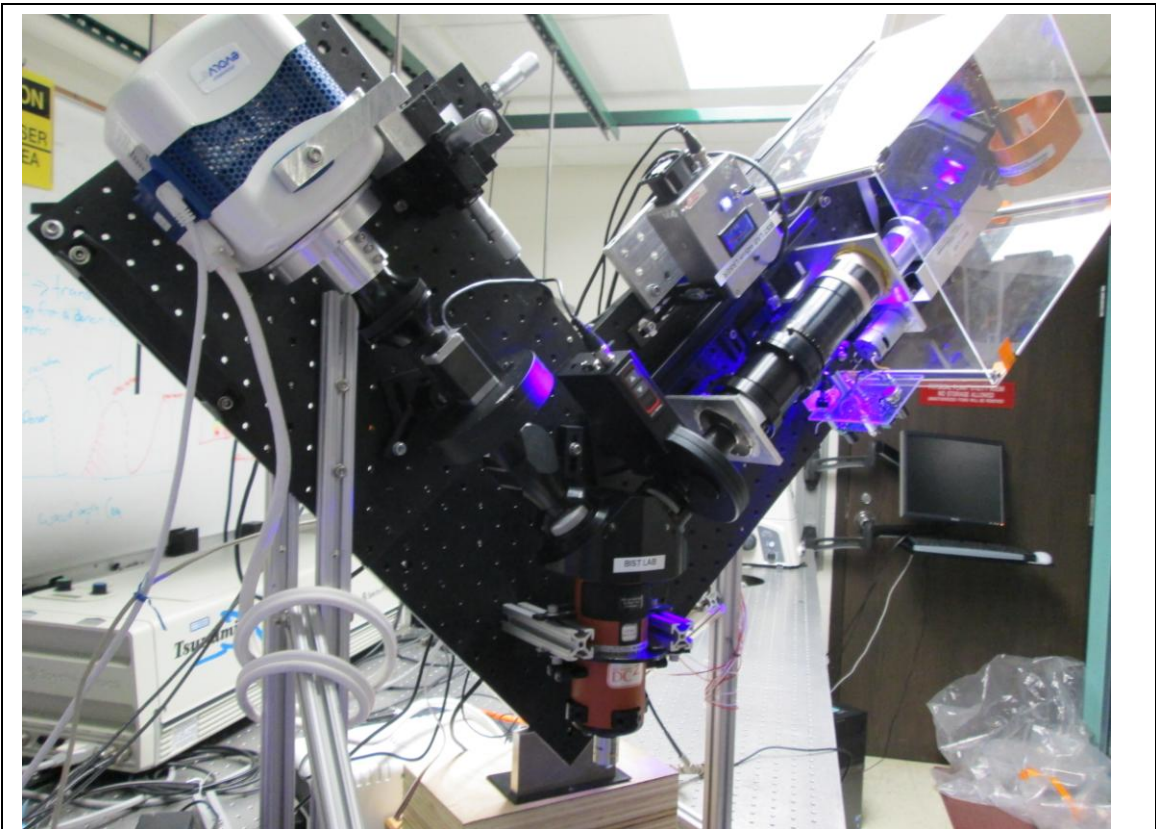
Figure 10 - Image of the Optogenetic Brain-Machine Interface, designed and implemented in the BIST (Biological Sciences and Technologies) Lab at the University of Wisconsin-Milwaukee, ready for experiments at the LOCI (Laboratory for Optical and Computational Instrumentation) lab at the University of Wisconsin-Madison

of interest using the spatial light modulator (DMD) and simple geometric relations between the imaging and projection paths. An actual image of the device is presented in Figure 10.

In order to test the projection and imaging resolutions of the optogenetic BMI, along with a BIST lab coworker (Ryan Falk), we used the 1951 Air Force Resolution Target (Edmond Optics, Catalog # NT58-198) to measure the resolution of the imaging path. By projecting a uniform pattern of blue light from the DMD and imaging the fluorescence given off by the Resolution Target we were able to determine the imaging path to have a resolution of approximately 4.38 micrometers [35]. In order to measure the projection path's resolution, we uploaded and projected an image of the air force target onto a uniform fluorescence sample then we recorded the fluorescence signal through the imaging path. Using both the image captured by our camera, the size of the image uploaded to the DMD and the BMI's magnification, we were able to determine a projection resolution of approximately 4.9 micrometers. The recorded images during this process are shown in Figure 11.

Figure 11 - A) The imaging path resolution. Here we imaged the Resolution Target by projecting a uniform pattern of blue light via the projection path and recording the fluorescence signal. B) The projection path resolution. Here we projected an image of the Resolution Target onto a uniform fluorescence sample and recording the fluorescence signal using the BMI's imaging path.

A

B

Figure 12 - Demonstration of projection resolution and the quality of the imaging path. A) Mask for the projected image. Blue projection light will reflect off of the white areas towards the telecentric lens and the black areas will be reflected away from the telecentric lens. B) The mask is being projected onto a YFP+ brain slice fixed on a microscope slide.

To demonstrate the combined projection and imaging capabilities of the device, we have modulated our optogenetic excitation light to project a masked pattern onto a YFP+ brain slice fixed on a microscope slide using a 4X microscope objective. Then, we imaged the fluorescence emission light with our EMCCD camera. See Figure 12 for the projection mask displayed on the DMD and the resulting fluorescence image.

Figure 13 - A) An approximate drawing of the image which is projected onto a uniform sample during the registration process. Using geometry, the DMD coordinates of the four projected spots or corners, and the captured image for the imaging path (B), we can make a close approximation as to the locations of objects in images captured by the camera. This is how targeting of specific areas or combinations of areas possible with our system.

The programming which links many devices together to function as one finely tuned device for complex optogenetic investigation of neural circuits was programmed using LabView and Matlab. One notable program is part of a process called "Registration" which makes geometric relationships between the camera pixels and the DMD pixels. Figure 13(A) is an approximate drawing of the image which is projected onto a uniform sample during the Registration process. Using geometry, the DMD coordinates of the four projected "spots" or "corners", and the captured image from the imaging path, Figure 13(B), we can make a close approximation as to the locations of

objects in future captured images. This is how we have made targeting of specific areas or combinations of areas within the camera's field of view possible.

Figure 14 demonstrates the targeting ability of the optogenetic BMI. Demonstration of automatic cell detection made possible by the registration process which, using geometry and known projection masks, relates the camera pixels and the DMD pixels. Figure 14(A) shows the imaged fluorescence signal from a pollen grains sample while projecting a uniform projection pattern from the DMD, see Figure 14(C). We then use a filtering code on the image in Figure 14(A) to automatically extract the "objects" and generate an appropriate patterned DMD projection image using the previously mentioned registration process which, as we can now see, provides the basis for targeting objects in the field of view. Figure 14(C) shows a uniform DMD projection pattern while Figure 14(D) shows a patterned DMD projection image which is built to target the objects within the field of view optogenetic stimulation light using data from the Registration process, see Figure 14(B).

Figure 14 - Demonstration of automatic cell detection made possible by the registration process which, uses geometry and known projection masks to relate the camera pixels and the DMD micromirrors. (A) Fluorescence images of pollen grains while projecting a uniform pattern with the DMD (C). (B) Using a filtering code, we automatically extract the "objects" from the image in part (A) and generate an appropriate projection pattern (D). The generation of the projection pattern requires the DMD to camera registration data.

Figure 15 - Current block diagram which was used in the experiments which will be discussed in chapter 4.

The current block diagram for our optogenetic Brain-Machine Interface is

displayed in Figure 15. Beamsplitter #1 and #2 can be customized for various experiments

which may use different opsins or fluorescence indicators. The camera and DMD can be

easily related to each other allowing the targeting of areas of interest. We have

demonstrated the feasibility of incorporating fiber bundles directly after the objective lens

through various experiments. In Figure 16(left) we see the projection image from the

DMD through a bundle of 16,000 optical fibers. In the same figure (middle) the same

fiber bundle is shown sitting next to a mechanical pencil for size comparison. If we

increase the magnification of the external CCD, which is imaging the fiber bundle tip, we can see the individual fibers. Attempting to image fluorescence through a fiber bundle is difficult since the fluorescence signal is faint. One idea to overcome this obstacle is to use a graded-index (GRIN) technology along with a spherical lens to provide a large numerical aperture (NA) while keeping loss of resolution to a minimum. In general, the larger the NA of a lens the more light it will be able to gather.

Figure 16 – Left: An image captured from a DMD projected pattern through a fiber bundle which consists of 16,000 optical fibers. Middle: Size comparison image of the fiber bundle and a mechanical pencil. Right: A magnified image taken of just the wheel. If you look closely you can see the individual fibers.
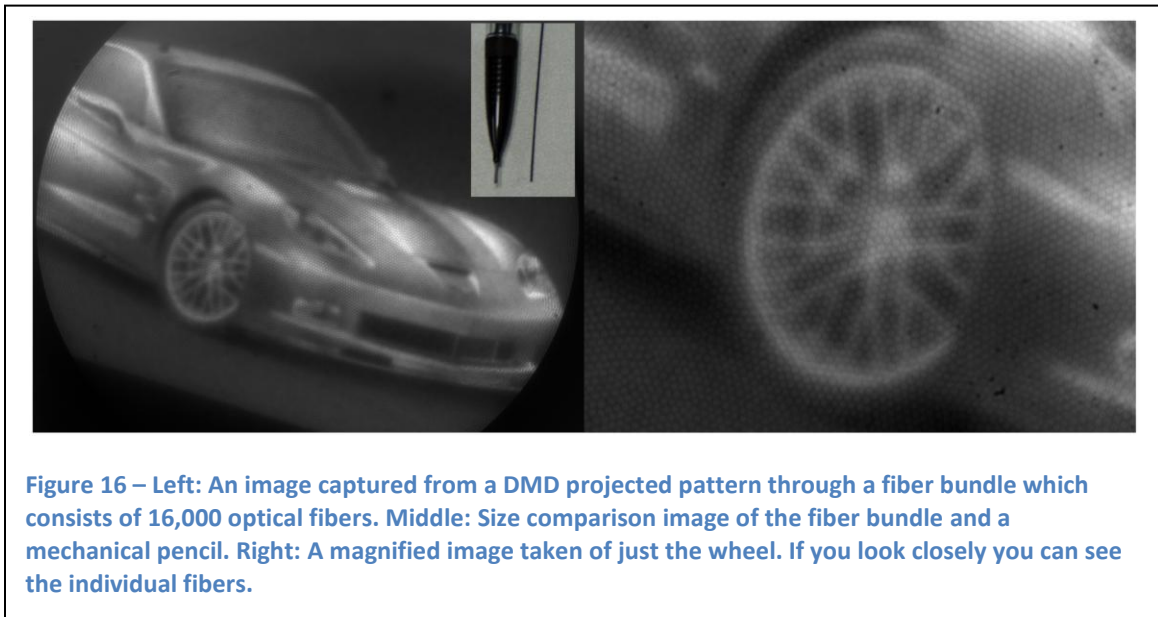
4. Micro-ECoG

Our collaborators at NITRO (Neural Interface Technology Research and Optimization) lab at the University of Wisconsin-Madison, microfabricate custom micro-electrocorticography (micro-ECoG) electrode arrays for measuring the cortical local field potentials created by the optogenetic patterned stimulation. Micro-ECoG arrays are implanted on top of the dura matter and are therefore useful for localizing cortical activity across the surface of the brain. Researchers at NITRO used photolithography to define 16 platinum electrode sites (150 μm diameter) in a 4x4 grid (0.5 mm site-to-site spacing).

They selected Parylene-C, a transparent biocompatible polymer, as the electrically insulative substrate, so that photostimuli could be applied to the cortex through the transparent device. In chapter 4, we will be discussing many experiments which combine both the custom designed micro-ECoG arrays and the custom built optogenetic neural modulation DMD platform.

Chapter IV.   BMI Experiments and Results

1. Optogenetic Neural Modulation and ECoG Recording

Our first experiments were designed with the intent to investigate the spatial and temporal capabilities of the optogenetic BMI setup by applying a photostimulus to the pyramidal cells in the cortex of a ChR2 positive transgenic mouse while monitoring the effect on the local field potentials using the NITRO's micro-ECoG array with a 3kHz sampling frequency. NITRO's micro-ECoG array employs platinum electrodes on a biocompatible transparent parylene-C substrate which allows our custom built fluorescence microscope to image the fluorescence signals from the brain tissue underneath the ECoG. Our collaborators at NITRO lab fabricated the electrode arrays on a transparent insulative polymer so that when implanted on top of the dura and under a cranial window, photostimuli could still be patterned on the cortex [17]. To investigate the spatial functionality of our optogenetic BMI device, we varied two spatial parameters, the location and the area of the photostimulus, while keeping temporal parameter, photostimulus duration, at 4 ms. In order to investigate the temporal potential of our optogenetic BMI device we varied the photostimulus duration while keeping spatial

parameters constant. We have employed a digital micromirror device that allows us to keep the optical power constant per area and unit of time. Keeping the optical power constant per area and time is important when attempting to quantify the stimulation caused by a varying photostimulus.

A. Spatial Experiments

We have projected Optogenetic photostimulus patterns with both varying area and location on the cortical areas of Thy1:ChR2/H134R-YFP mice while monitoring the local field potential (LFP) changes using NITRO's micro-ECoG array. These first experiments were conducted to better understand the spatial distinction of the LFP changes caused by the spatially varying photostimulus. We projected many different shapes as well as complex patterns of photostimulus with which we avoided the location where the micro-ECoG electrodes and leads were located. The electrode array is connected to a high-impedance low-noise amplifier and voltages are recorded referenced to a coil wire implanted in the contralateral cortical hemisphere and averaged over 100 trials. In these experiments, the cortex is stimulated by 8ms pulses of blue light produced by a 445nm laser module which provides $4.5mW/mm^2$ optical power density and 2Hz repetition rate.

a. Results

Figure 17, displays the mapped cortical potentials which were evoked optogenetically with varying spatial parameters. The potentials were of greatest amplitude near the photostimulus location, suggesting that photostimulus-correlated activity is primarily colocalized with the photostimulation location. Stimulating larger cortical volumes, Figure 17(B), induced similar amplitude potentials which were spread over a larger cortical area. In Figure 17, we have attempted to make visualization of the

electrode data easier to digest by using a color-mapping system, or heat-maps, which uses colors to help the reader visualize the spatial distribution of LFPs measured during these experiments. The localization heatmaps in Figure 17 were generated with the spline interpolation command of Matlab.

Figure 17 – Visualizations of ECoG's electrical LFP measurements during spatial experiments. On left, an image of the implanted ECoG overlaid with a blue square which represents the photostimulus size and location, the white lines are the electrode measurements, and the light blue line represents the stimulation duration. On the right, the circles represent electrodes, the blue squares represent photostimulus size and location, and the background is a color interpolation. Dark red equates to a larger LFP and white represents a smaller LFP. From the data, we can visualize the effects of translating the photostimulus as well as scaling the photostimulus size. Figure also used in [64]

B. Temporal Experiments

In order to understand how the local field potentials (LFP) change with respect to temporal variations, we have projected optogenetic photostimulus patterns with varying photostimulus duration while monitoring the LFP changes using a micro-ECoG array. The temporal experiments were conducted to better understand the temporal distinction of the LFP changes caused by varying the duration of a photostimulation. We chose three temporal photostimulus durations: 4ms, 8ms, and 24ms.

a. Results

In Figure 18, we can observe the mapped cortical potentials which were evoked optogenetically with varying photostimulus durations. The LFPs increased in amplitude as the photostimulus duration was increased. Along with this increase in amplitude, the LFPs remained elevated for a longer period of time.

C. Spatial and Temporal Experiment Controls

In order to verify that, indeed, the effect observed by the micro-ECoG array was caused by the light activation of the ChR2 ion channels, we ran control experiments. Having identified the photoelectric effect as a possible artifact which may affect our data we decided to run two experiments to help rule out this artifact or show that its effect is negligible while implanted on the cortex of a mouse. One control experiment, see Figure 19, involved implanting wild type mice with electrode to understand the effect a photostimulus had in mice which have not been transfected with ChR2 light-gated ion channels. The previous experiments conducted by the NITRO lab at the University of Wisconsin-Madison studied the photoelectric effect of their transparent micro-ECoG while it was submerged in saline solution. Their results concluded that the photoelectric

Figure 18 – A visualization of the temporal experiments using the optogenetic brian-machine interface. On the right, we establish the absolute location of the electrode array, photostimulus, and camera's field of view with respect to the animal's head. On the left, we can see the photostimulus' size, shape, and location (light blue square), the electrodes measured LFPs (red, green, and blue lines), the start of the photostimulus is located at the blue dot, and the photostimulus duration is represented by the varying colors. The blue color is the LFP of the 24 mS duration, the green is the LFP of the 8 mS duration, and the red is the LFP of the 4 mS photostimulus duration.

peak was around 5 microvolts which is substantially less than the LFP recorded during

optogenetic photosimulation during our experiments; see Figure 19. Another control

experiment consisted of avoiding the electrode sites and leads with the projection light;

see Figure 20. From the micro-ECoG readings, it is clear that any artifact which may be

caused by shining light onto the micro-ECoG is negligible. The micro-ECoG

measurements and stimulation pattern projected while avoiding the micro-ECoG

electrode sites and traces are in Figure 20. These results show that the recorded potentials

were nearly the same or negligibly different, ruling out the photoelectric effect as a

substantial contributor to the results obtained.

Figure 19 – Shows the control experiments ran for the NITRO's transparent micro-ECoG electrodes. A) We demonstrate the comparison of micro-ECoG measurements in-vivo between a ChR2 positive mouse and a wild-type mouse. This micro-ECoG data clearly shows that the electrode response in the ChR2 positive mouse is greater than that of the wild-type mouse. B) Demonstrates the photoelectric effect of the micro-ECoG in-vitro in saline solution with varying photostimulus duration. We can see that the effect is dependent on the duration of the photostimulus but that the electric response is orders of magnitude smaller than what is recorded in ChR2 positive mice. Figure adapted from [54]

Figure 20 – A direct comparison of a photostimulus pattern which projects on the micro-ECoG implant and a pattern which avoids the electrodes and leads of the electrodes with the photostimulus excitation light. A) An image of the photostimulus for the solid projection. B) An image of the photostimulus projection which avoids the electrodes and leads of the electrode. C) Micro-ECoG LFP measurements where the green lines represent the solid projection and the yellow lines represent the masked projection which avoids the micro-ECoG electrodes. Using this data, we can see that the effect of avoiding the electrodes has only a small and insignificant effect on the local field potentials. Figure adapted from [40]

2. Closed-Loop BMI using Projection Path and micro-ECoG

It's easy to imagine the potential impact of having the ability to modulate neural activity using feedback from a reference signal. The reference signal could be the brain activity, blood flow, metabolic activity, or even the signal from a sensor which is replacing a damaged sensing organ. For example, closed-loop strategies could be beneficial in possible treatments of seizures which are an event of abnormal, unsynchronised discharge of cortical neurons [36]. Imagine recording from an area of the brain tissue known to have abnormal activity discharges while having the ability to inhibit the abnormal action potentials within these seizure areas as they become overactive. Imagine that important connections within the brain are disconnected due to an event such as brain injury or a stroke. Could it be possible to reconnect these areas using a device which can modulate one area of the disconnected tissue according to the monitored activity of the other disconnected tissue area? Feedback is a necessary component of a BMI algorithm which intends to finely adjust the activity of neurons in the area of interest within the brain. During the following experiments, we adapted such a feedback system using micro-ECoG readings for neural monitoring and our optogenetic BMI platform for neural modulation.

This section consists of two experiments in which we explore two types of closed-loop functionality that are potentially valuable for future BMI devices: simultaneously controlling the activity of many areas of tissue independently and creating an "Artificial Connection" between two areas which otherwise would have minimal neural interaction by utilizing the spatial and temporal capabilities of the BMI.

A. Micro-ECoG Feedback Mechanism

The feedback mechanism employed throughout the closed-loop experiments consists of a simple negative feedback loop described in Figure 21. The most critical parameter of the feedback mechanism is the proportionality factor, K_p. K_p is the scaling factor for the time duration of the stimulation signal projected onto the tissue from the DMD device. Using this simple feedback system, we were able to conduct a few closed-loop experiments which monitor the local field potentials using the micro-ECoG from NITRO's lab and stimulating the pyramidal neurons in the cortex of transgenic mice using our custom built DMD neural modulation platform. In Figure 22, we examine the

Figure 21 – A) A schematic of the closed-loop brain-machine interface algorithm. This closed-loop system works by introducing an optical neurostimulating signal using the brain-machine interface and uses NITRO's micro-ECoG electrodes to measure the LFPs of differing areas of tissue. This measurement is compared to a set-point and then an error signal is sent to the DMD in the form of a analog voltage which is related to a specific photostimulus duration. B) Shows the exact algorithm used in our closed-loop brain-machine interface. Figure adapted from [64]

consequences of varying the value of the proportionality constant.

Figure 22 – An experiment which demonstrates the effects of varying the proportionality constant (K_p). The top graph shows the ECoG measurements (in green), set point (in blue) with respect to time which is the bottom axis of all graphs. The middle graph shows the duration of each photostimulus at each time. The bottom graph displays the value selected for each K_p variable at each time. In the top graph, we can see instances where the system is underdamped (0 s to ~250 s), overdamped (~250 s to ~350 s), and critically damped (~350 s to ~450 s). Figure adapted from [64]

B. Multiple Area Independent Modulation

The motivation for conducting this experiment is to demonstrate an ability to increase the neural activity of four areas by varying the photostimulus duration according to the previous sequence's electrode signal at each location. This experiment can be viewed as a precursor to more complicated experiment where activity levels over space are kept at their variable set points throughout time. In these experiments, we hope to create patterns of activity that are variable over time and space resembling the recordings from fMRI. Due to current digital signal processing limitations, we could only read and filter neural signals from 4 electrodes during this experiment thus limiting the number of electrodes that could be observed in real-time.

Figure 23 – Visualization of a complex spatio-temporal closed-loop neuromodulation experiment. The upper left image shows the location of the photostimulus (the black square) and the photostimulus' related electrode number. The bottom row, which consists of three images, is the temporal sequence of applied photostimulus projection locations. The sequence of masks applied is as follows, projection mask #1 is available for projections for 100 ms, then projection mask #2 is available for projections for 100 ms, then projection mask #3 is available for projections for 100 ms, followed by a period of 700 ms when no projection mask is available for projection. This sequence is repeated for hundreds of seconds, data of which is displayed in the top right image. The top right image shows the measaured micro-ECoG values (in green) of all four electrodes involved in the closed-loop experiment, the activity set-point (in blue) for each of the four electrodes, and the photostimulus duration (in red), all through time which is the horizontal axis of the graphs. From this data, we can see that our spatio-temporal BMI has the ability to control multiple points which follow independent set-points over time. Figure adapted from [64]

The multiple area independent modulation experiment was designed to modulate

the activity of 4 areas of tissue around electrodes from the base level activity to

independent pre-chosen neural activity set points (see Figure 23) using feedback from

each electrode recorded during the previous stimulation sequence. The feedback signal

allows the adjustment of our photostimulus duration, either longer or shorter, according

to the reference set points. Using feedback, we were able to raise the level of activity to

the set point level within a relative proximity of its associated set points by adjusting the

feedback parameters (see Figure 23).

Figure 24 – (Top Image) An image visualization of the 4 point closed-loop BMI experiment. This image consists of an intensity color (black equals little to no activity while white equals most increased activity) for all 157 sequences of the experiment. The electrodes which correspond to a given photostimulus are identified by the red rectangles and the square # located to the right of the image. The middle image is a visualization of the projection sequences. The bottom diagram is a block diagram of the electrode signal filtering and processing.

C. "Artificial Connection" Between Two Neural Areas

The "artificial connection" experiment which I present is motivated by the ability to connect two "sites" of the brain tissue which otherwise would not have been connected or have been disconnected due to brain injuries or diseases. In Figure 25(a), we can view the physical location of the two sites which we intend to "connect". The two sites are placed sufficiently far away from each other to minimize the cross talk of the local field potentials picked up by the micro-ECoG electrodes. The procedure for this experiment is as follows: Site 1 is programmed to follow a predetermined electrode activity set point where the tissue's activity is modulated by the optogenetic DMD stimulation platform and the feedback system with a proportionality factor (K_p) the same as described earlier in the multiple area independent modulation experiment. Site 2 is programmed to follow the electrode measurement of site 1's activity caused by the previous stimulation. This essentially creates an artificial connection between these previously minimally connected areas of cortical neural tissue.

Looking at Figure 25(b), we can observe the electrode measurements at site 1 and site 2 as well as the activity set point of site 1. While observing the results in Figure 25(b), it shows that the site 1 (blue line) roughly follows the set point (black line), and we also see that site 2 (green line), slightly lags, or follows site 1's LFP measurement (blue line).

Figure 25 – The "artificial connection" experiment. This experiment is an experiment which was run to grasp the feasibility of bypassing nonfunctioning tissue within the cortex. In this experiment, we used a feedback system where the electrode measurements controlled the projection durations of photostimulus. The overall process is as follows: Site 1 is programmed to follow the set-point and site 2 is programmed to follow the electrical activity measurements from the electrode located at site 1 thereby allowing the activity signal from site 1 to be transferred to site 2 without these two locations being previously associated with each other. (b) It can be observed that the activity of site 1 follows the set-point, while site 2 slightly lags the activity of location 1 or location 1 follows the electrode measurements from location 2. This figure is adapted from [64]

3. Optogenetic Investigation of Neurovascular Coupling

The experiments we designed to investigate the causal relationship between neural activity and hemodynamics within brain tissue are of clinical and experimental interest. Optogenetics is a great tool to investigate this relationship. A temporal correlation has been established between LFPs and the BOLD signal recorded by fMRI machines [37]. Another interesting result in using optogenetics to investigate the relationship between neural activity and hemodynamics is to understand how optogenetic stimulation relates to hemodynamics. Benefits of using the custom projection device and optogenetics to investigate hemodynamics is the cell type specificity and a direct route to recruiting activity as well as the spatial patterning of stimulating light. Blood flow changes in response to optogenetic stimulation have been previously described [38]. This experiment provides a novel approach for studying neurovascular coupling by imaging

cerebral blood vessels in-vivo while applying photostimulation to the cortex through a thinned-skull window in Thy1-ChR2/H134R mice [39] using the previously described optogenetic projection device, see Figure 15, and an intravenal dye, Rhodamine B isothiocyanate-dextrane (Sigma, 70 kDa). For more specifics on the animal protocol refer to [40].

A. Experimental Procedure

Epifluorescence images of the cortical surface were collected at 7 frames per second. Mirror #1, see Figure 15, was a dicroic with longpass cutoff at 500 nm. We used a 50%-50% beam splitter for mirror #2. Rhodamine B was excited with green light (550/40 nm, 1 mW total power) from a xenon light source (DG-4, Sutter) and a red emission filter 630/50 nm (Chroma) was positioned in front of the camera. During each trial, the vessels were imaged for 10 seconds prior to the photostimulus and 30 seconds following the stimulus. The photostimulus (4.5 mW/mm^2, 445 nm) was applied for 1 second and pulsed at 25 Hz (20 ms on, 20 ms off). Trials were repeated every 1 to 2 minutes, and 7 trials were done for each photostimulus pattern.

To determine vessel diameters, measurement locations were specified on each vessel manually and a band was defined along the axis of the vessel over which the data were spatially averaged. The vessel width was measured as the full width at half-maximum, and a 3 point median filter and 3 Hz low pass filter were applied similar to Drew et al. [41].

B. Results

Branches of the middle cerebral artery (MCA) dilated transiently following

photostimulation (25 Hz x 20 ms for 1 second, 4.5 mW/mm^2, 445 nm) of the cortex, see

Figure 26 – Quantification of blood vessel diameter expansion in response to optogenetic photostimulus in ChR2 positive mice. Three spatially varying photostimulus masks were used to stimulate the cortical neurons within a mouse (a-c, overlaid in blue). The photostimulus was applied as a pulse train with irradiance held constant (20 mS pulsewidth at 25 hz for 1 Sec, 4.5 mW/mm2, 445nm wavelength). The average image of prestimulus recordings is shown as the gray image and the post stimulus percent change overlaid in red (a-c). From this data, the large (a) and medium (b) photostimuli caused the middle cerebral artery branches to dilate, while the veins showed minimal response. (d) Arteries are labeled a1 and a2 while veins are labeled v1 and v2. (e) Measured diameter values of the middle cerebral artery branches (a1 and a2) showed a 30% increase following the large area photostimulus, while the medium area photostimulation caused a 15% diameter increase, and the small photostimulus caused minimal dilation. In comparison to the arteries, the venous response (v1 and v2) was smaller and seemed to return to basil value slower. Seven trials of each stimulus were conducted per animal. (f) The study was replicated in 4 ChR2 positive mice and 4 wild type mice, and the median percent change of the MCA was significantly larger (p = 0.014) in the ChR2 positive mice than in the wild type at the alpha = 0.05 confidence level (one-tailed signed rank test). Figure adapted from [40]

Figure 26, recovering to prestimulus diameters after several seconds. The hemodynamic response was robust, occurring in every individual trial. While branches of the MCA dilated more than 30% for the large photostimulus, nearby veins showed a much smaller and somewhat delayed response.

The magnitude of both the arterial and venous response depended on the cortical area excited optogenetically. We used the microprojector to create photostimulus patterns of different areas while holding optical power per area (irradiance) constant. The smallest photostimulus evoked little to no hemodynamic response, while the two larger photostimulus patterns evoked proportionate responses.

C. Neurovascular Coupling Control Experiments

As light is absorbed by tissue, there is a transfer of energy in the form of heat. There were concerns that this increase of tissue temperature could have introduced an artifact. Also, some fMRI artifacts have been reported in wild-type (WT) rodents at high photostimulus levels [42,43]. In response to these concerns, we replicated our study in both ChR2 expressing (n=4) and WT (n=4) mice, Figure 27. The median arterial response to the large photostimulus was significantly (p=0.014) larger in ChR2 than WT mice, see Figure 26 and Figure 27.

Figure 27 – Quantification of blood vessel diameter expansion in response to optogenetic photostimulus in wild type mice. Three spatially varying photostimulus masks were used to stimulate the cortical neurons within a mouse (a-c, overlaid in blue). The photostimulus was applied as a pulse train with irradiance held constant (20 mS pulsewidth at 25 hz for 1 Sec, 4.5 mW/mm2, 445nm wavelength). The average image of prestimulus recordings is shown as the gray image and the post stimulus percent change overlaid in red (a-c). From this data, there was a relatively small arterial diameter increase for all sizes of photostimulus and the veins showed no change. (d) Arteries are labeled a1 and a2 while veins are labeled v1 and v2. (e) A small artifact was observed following the photostimulation, but the aplitude was always much smaller in wild type than in ChR2 positive mice (see Figure 26). Figure adapted from [40]

We utilized the full capacity of the microprojector to investigate whether direct photostimulation of the major cerebral vessels is responsible for the hemodynamic response, see Figure 28. We explored this potential artifact, because if perivascular nerves express ChR2, then a direct cholinergic mechanism could explain the optogenetic hemodynamic response. We applied a solid photostimulus pattern, Figure 28(a), and a

pattern with the major cerebral vessels removed, Figure 28(b). The resulting

hemodynamic responses, Figure 28(d), were similar. Had perivascular nerves been

involved, we would have expected a disproportionately smaller hemodynamic response

for pattern with vessels omitted. These experiments, see Figure 28 andFigure 29, suggest

that projection is necessary for observed hemodynamic response, and direct projection

onto the measured vessels cannot account for the observed hemodynamic response.

Figure 28 – Quantification of artifacts caused by projecting high intensity laser light directly onto the blood vessels. (a) We projected a solid square and (b) a pattern where the blood vessels' locations were masked. Other photostimulus parameters were 20 mS pulsewidth at 25 hz for 1 Sec, 4.5 mW/mm^2, 445 nm were held constant. The blood vessels were measured at the locations labeled (a1, a2, v1, and v2) in (c). (d) The hemodynamic response was similar for the solid and masked photostimulus patterns. Figure adapted from [40]

Figure 29 – Quantification of diameter size comparing normal projection using the optogenetic brain-machine interface and a blank projection (or no projection) with the optogenetic BMI. The blood vessels show no change with the DMD chip projecting no mask while the high powered laser is still operating. This basic control demonstrates the necessity of providing blue light to the cortex to have an optogenetic response. Figure adapted from [40]

4. Optogenetic Investigation of Neurometabolic Coupling

A. Experimental Procedure

We imaged NADH (nicotinamide adenine dinucleotide) fluorescence intensity using standard (single photon) excitation. NADH has an excitation peak near 350 nm and an emission peak near 450 nm. We used extremely low levels of UV (ultra violet) light to minimize UV damage to the cortex and to avoid excitation of ChR2. 8 $\mu W/mm^2$ has been suggested previously as a safe level for prolonged in-vivo NADH imaging [44]. We used a UV LED (365 nm, Thorlabs) and an OD1 neutral density filter (Thorlabs) to reduce the light level to 8 $\mu W/mm^2$. At this level, we observed no photobleaching of NADH, and the light intensity is orders of magnitude below what could possibly excite ChR2. Using the EMCCD camera made the imaging of such a faint signal possible.

B. Results

We imaged NADH fluorescence intensity as a signature of the metabolic status of the cortex following ChR2 photostimulation (445 nm, 4.5 mW/mm^2, 5 ms x 66 Hz for 1 second). When oxidized, NADH, an endogenous fluorescent protein involved the citric acid cycle, glycolysis and other metabolic pathways, becomes NAD+, which doesn't fluorescence. The NADH signal decreased by about 4% following photostimulation and it recovered over several seconds, see Figure 30.

This effect was not observed in WT mice; see Figure 30(g) and Figure 31. Similar to the vascular experiment, the peak amplitude of the NADH response depended on the area of stimulation.

Figure 30 – Metabolic increase following ChR2 photostimulation. Nicoadenine dinucleotide (NADH) is involved in cellular metabolism. When cell metabolism increases, NADH is oxidized to NAD+. NADH fluoresces while NAD+ does not. In this experiment, we imaged this fluorescence signal before and after ChR2 stimulation (5 mS pulsewidth at 66 hz for 1 second, 4.5mW/mm^2, 445 nm) of different cortical areas. A large decrease in the fluorescence signal (f) of the region of interest (ROI) displayed in (e) for the large stimulus area (d) while for the smaller photostimulus area (a) there was a smaller response (c) within the ROI (b). 10 trials were conducted for each photostimulus pattern per animal. The study was replicated in 3 ChR2 mice and 3 wild type mice with the peak fluorescence change for the large photostimulus plotted in (g). A p-value of 0.05 was found for a one-tailed signed rank test. Figure adapted from [40]

Figure 31 – Control data for the NADH experiments using wild type mice. While projecting a small (a) of large (d) photostimulus onto the cortex of wild type mice there was no changed observed in the NADH fluorescence intensity (c) and (f). Blood vessels were excluded from the ROIs (b) and (e). Figure adapted from [40]

Chapter V. Predicting Light Distribution within the Brain Tissue

1. Motivation

Using light-gated ion channels in optogenetic neuromodulation allows for unprecedented spatial and temporal control of the activity of neural tissue within cortical areas of the brain. It is known that these optogenetic light-gated ion channels require adequate optical stimulation to cause neural spiking. Therefore, it is essential to have the ability to predict light intensity distribution within tissue. It is important to determine, given some optical input, which areas of tissue could receive adequate optical stimulation power to cause an optogenetic reaction. It is also important to determine which areas will receive inadequate optical power to cause an optogenetic reaction. Another important consideration, while using optogenetics, is limiting optical stimulation power to levels below the photo-bleaching or photo-damage threshold of the tissue. Finally, it is known that biological mediums, such as the brain tissue, are inhomogeneous, turbid, and anisotropic which introduce problems with the assumption that the tissue is homogeneous or isotropic.

With these considerations in mind, we have developed a procedure to extract the optical properties of rat brain tissue. With these optical properties, we assembled a 3-D tool with which investigators could run Monte-Carlo simulations to determine the optical distributions within the brain tissue before applying optical neuromodulation. This enables them to ensure that they are not damaging tissue in the stimulation area, that they are applying adequate stimulation power to the targeted area, and also allows them to knowingly avoid stimulating volumes of the brain tissue deemed necessary to avoid.

2. Custom Device for Extraction of Optical Properties in Brain Tissue

The optical properties of the brain tissue are typically described in publications by three variables: the absorption coefficient, the scattering coefficient, and anisotropy factor [45]. In order to calculate the optical properties of the tissue, we need to measure three values from voxels within the volume of brain tissue. These measurements include ballistic transmittance, diffuse reflectance, and diffuse transmittance [46]. The diffuse reflectance and diffuse transmittance measurements were aquired simultaneously using setup #1 in Figure 32 which uses two integrating spheres. This is a standard for acquiring these measurements [47]. The ballistic measurements were obtained using the setup #2 described in Figure 32.

Our approach for measuring the necessary data to calculate the optical properties of brain tissue required the following procedure. We scanned 500 micrometer thick slices of fresh Sprague-Dawley rat brain tissue at a resolution of approximately 3000 points per square centimeter for three different cuts (sagittal, transverse, and dorsal) and three different wavelengths (405 nm, 532 nm, and 635 nm). The three different cuts cover anisotropic factors and the three different wavelengths cover changes through the visible

spectrum. As fresh slices were cut with a vibratome (Lancer vibratome Series 1000), we immediately scanned the brain slices using setup #1. After scanning each slice, we covered them with a saline solution and placed them into a fridge to preserve them. After the whole brain was scanned, we transformed the scanning device to setup #2 and proceeded to re-scan each slice to obtain the ballistic transmittance data. When all three measurements were obtained, we used the inverse adding doubling (IAD) algorithm [46] to reconstruct the optical properties from the raw data. By mapping the optical properties to an atlas of the brain, a 3-D database of tissue optical properties was established. Next, using this 3-D database, we ran Monte Carlo analysis to simulate light-tissue interactions to determine the distributions of light within the brain tissue.

Figure 32 – Schematic of the experimental setups used to measure diffuse reflected and transmitted light (Setup 1), and the transmitted ballistic light (Setup 2). This figure is directly adapted from "Extraction of optical properties and prediction of light distribution in rat brain tissue." [65]

Figure 33 – The steps of Setup #2's procedure. Part (A) shows an image taken at the beginning of each ballistic experiment. Image processing is applied to the image to extract the slice. Software was developed to find which voltages to apply to the galvo mirrors which then are fed into scanning software. There are either 16 or 25 images taken during the scanning of each slice, see (B). Part (B) shows the ballistic data which is automatically extracted using developed software. All of the data for each slice is combined and interpolated to get an image, see part (C). Each successive slice can then be stacked to create a three dimensional database, see part (D).

3. Monte Carlo Light Distribution Simulations

In Figure 36, we ran simulations by employing our 3-D Monte Carlo toolbox [47,48] to demonstrate the effects of using different light delivery parameters such as the optical fiber diameter, wavelength, optical fiber numerical aperture (NA), and the beam profile of the light source, see Figure 36. We ran simulations using the Monte Carlo toolbox to present the impact on axial fluence at varying depths by placing an optical source at different locations on the cortex of the brain tissue. The simulation results are shown in Figure 35.
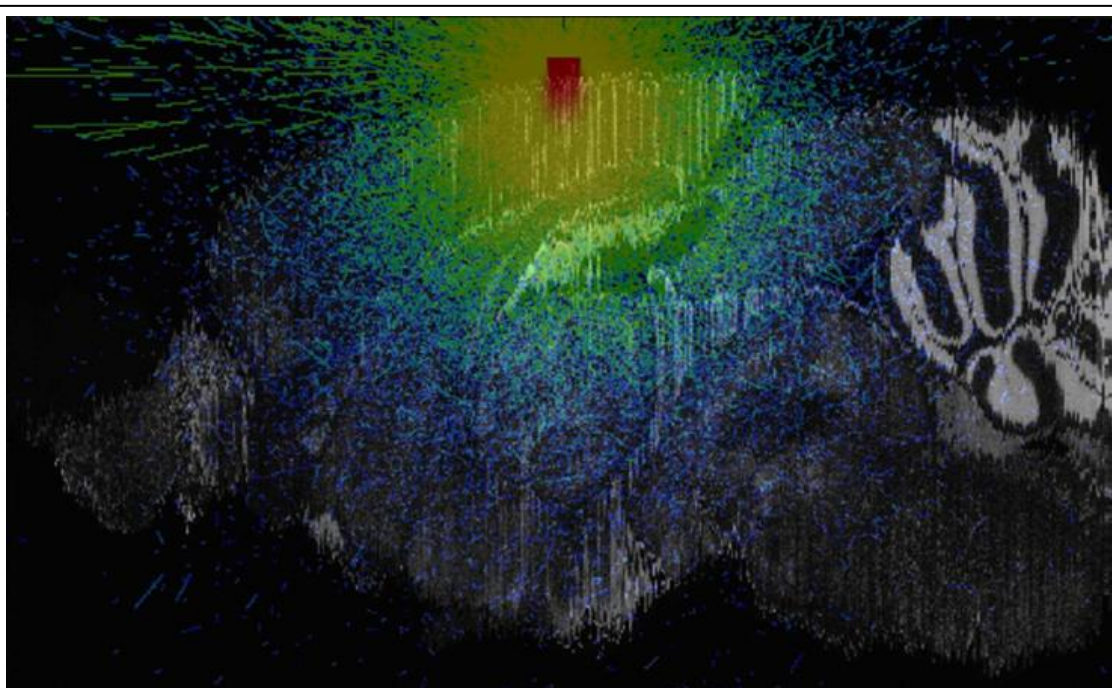
Figure 34 – A visualization of a Monte Carlo simulation overlaid onto the corresponding slice within a brain atlas.
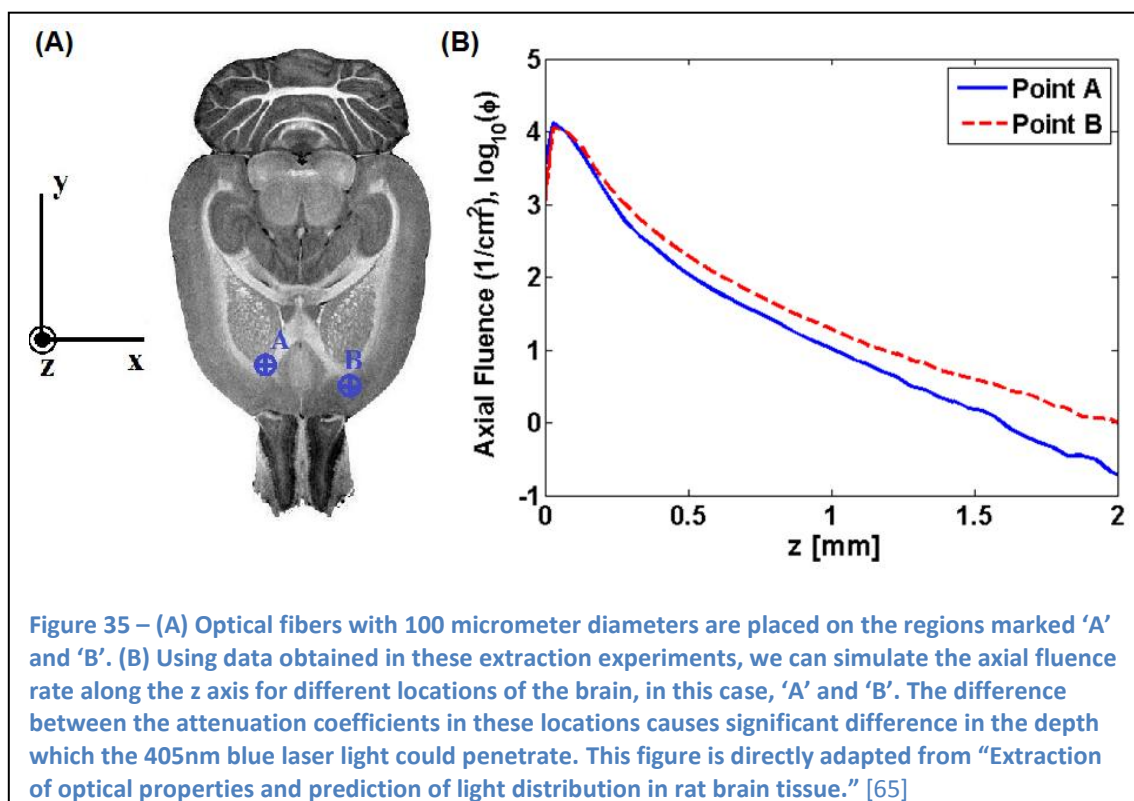
Figure 35 – (A) Optical fibers with 100 micrometer diameters are placed on the regions marked 'A' and 'B'. (B) Using data obtained in these extraction experiments, we can simulate the axial fluence rate along the z axis for different locations of the brain, in this case, 'A' and 'B'. The difference between the attenuation coefficients in these locations causes significant difference in the depth which the 405nm blue laser light could penetrate. This figure is directly adapted from "Extraction of optical properties and prediction of light distribution in rat brain tissue." [65]

Figure 36 – (A) shows the location an optical fiber which is being used as an input parameter for monte carlo simulatation software that implements our measured tissue properties which is used to investigate the effect of source parameters on the distribution of light within the brain tissue for 405nm laser light. (B) shows the effect of varying fiber diameters, (C) shows the effect of varying fiber numerical apertures (NA), (D) shows the effects of varying laser wavelengths, and (E) shows the effect of the beam profile on the axial distribution of light. This figure is directly adapted from "Extraction of optical properties and prediction of light distribution in rat brain tissue." [65]

Chapter VI.   Outlook for Optogenetic BMI devices and Experiments

1. Benefits of using light-gated ion channels for neuromodulation

Optogenetics has quickly become a well-known and widely used neuromodulation technique for the study of the nervous system in animal models. The success of optogenetics could be attributed to the large number of advantages this technique offers compared with classical techniques, such as chemical [50] and electrical stimulation [50,51]. The optogenetic technique allows for cell-type specific targeting [15] by using appropriate promoters. Another benefit of optogenetics is having the ability to bi-directionally control the cellular activity of neurons directly. By expressing both light-gated cation channels and light-gated anion pumps into neurons simultaneously, one can either increase or suppress neural activity [14,16]. Another benefit of using light for activating neurons lies within our technological tools which have been developed to manipulate light to form images or spatiotemporal patterns. As the design of these optogenetic BMIs are improved, they will play an important role in the development of complex experiments which add to our understanding of the brain. These devices will allow scientists to investigate neural circuitry in new ways and create complex treatments

for brain conditions where stimulation or inhibition is needed on the cortical surface. Examples of treatments where optogenetic BMIs could surpass current treatment technologies are allowing profoundly blind patient sight or enabling movement in severely immobilized limbs caused by brain malfunctions [53]. These deficits require complex neuromodulation in order to replicate the sensory input or the physical output of a normally functioning brain. Electrode arrays, which are currently being used for these purposes, have severe limitations which can be avoided by using optogenetics as the source of neuromodulation. As electrodes are implanted, they can cause a considerable amount of damage to the brain tissue. Limitations within the manufacturing process set limits on how many electrodes can be mounted onto a chip and how small the electrodes can be. In the next section I will introduce some light deliver systems which could be used in future optogenetic BMIs.

2. Future Optogenetic BMI designs and Experiments

There have been many light delivery mechanisms introduced as potential future

Figure 37 – Various techniques and devices developed or currently being developed to deliver light to areas within the brain in-vivo. (a) shows a basic implantation of a fiber optic in brain tissue in order to deliver therapeutic optogenetic light to areas deep within brain tissue. (b) shows a rat which has two implants. (c) shows the structure of a multichannel waveguide [57], and (d) shows an array of multichannel waveguides [56]. (e) shows a side-firing fiber which uses refraction to radiate light at near orthogonal angles (developed at BIST labs) [55]. (f) and (g) show a microactuator assembly which is able to translate optical fibers to different depths within brain tissue [55]. This figure is directly adapted from "Optogenetic brain interfaces." [54]

delivery mechanisms for varying experimental and procedural applications [54]. The simplest mechanism is a single optical fiber implanted stereotactically into target areas either shallow or deep within the brain, see Figure 37(a and b). By altering the tip of the optical fiber, one can direct the optical power nearly orthogonal to the fiber so that light is emitted in a side firing fashion, see Figure 37(e) [55]. This would be valuable where a treatment calls for stimulation or inhibiting light which is needed at different depths in the brain. Adding multiple optical fibers together or creating multiple channel waveguides introduces one could introduce different wavelengths in different areas or different depths [55,56]. This would be valuable where a treatment calls for differing stimulation or inhibiting light sources are needed at different depths or locations within the brain. Micro-actuator assemblies have been developed to move side firing fibers inside the brain in a direction perpendicular to the surface of the skull, see Figure 37(f and g) [55]. This device was designed to be used with some type of side-firing optical fiber so that one could modulate different layers within the brain.

Continuing to more complicated designs, we examine spatial light modulator (SLM) systems which include the device introduced in this thesis. Using these light modulating devices one can directly target areas on the surface of the cortex with great spatial and temporal resolution. As introduced in this thesis, one could develop a system which utilizes a DMD SLM, see Figure 38(a). Another SLM which was not introduced is liquid crystal technology which is fundamentally designed to be used with coherent light sources. These light modulators work by introducing a spatial phase shift which, in turn, introduces interference patterns creating spatially varying levels of optical power. For a simple block diagram of a liquid crystal design, see Figure 38(b). The block diagram

presented displays SLM systems which couple with fluorescence imaging systems to allow for monitoring of introduced opsins and/or monitoring the neural activity within the field of view. Advances in SLM technology could allow for the miniaturization of these designs allowing systems small enough to be feasibly implanted onto the surface of the skull allowing a patient the ability to be actively moving while wearing the optogenetic BMI device.
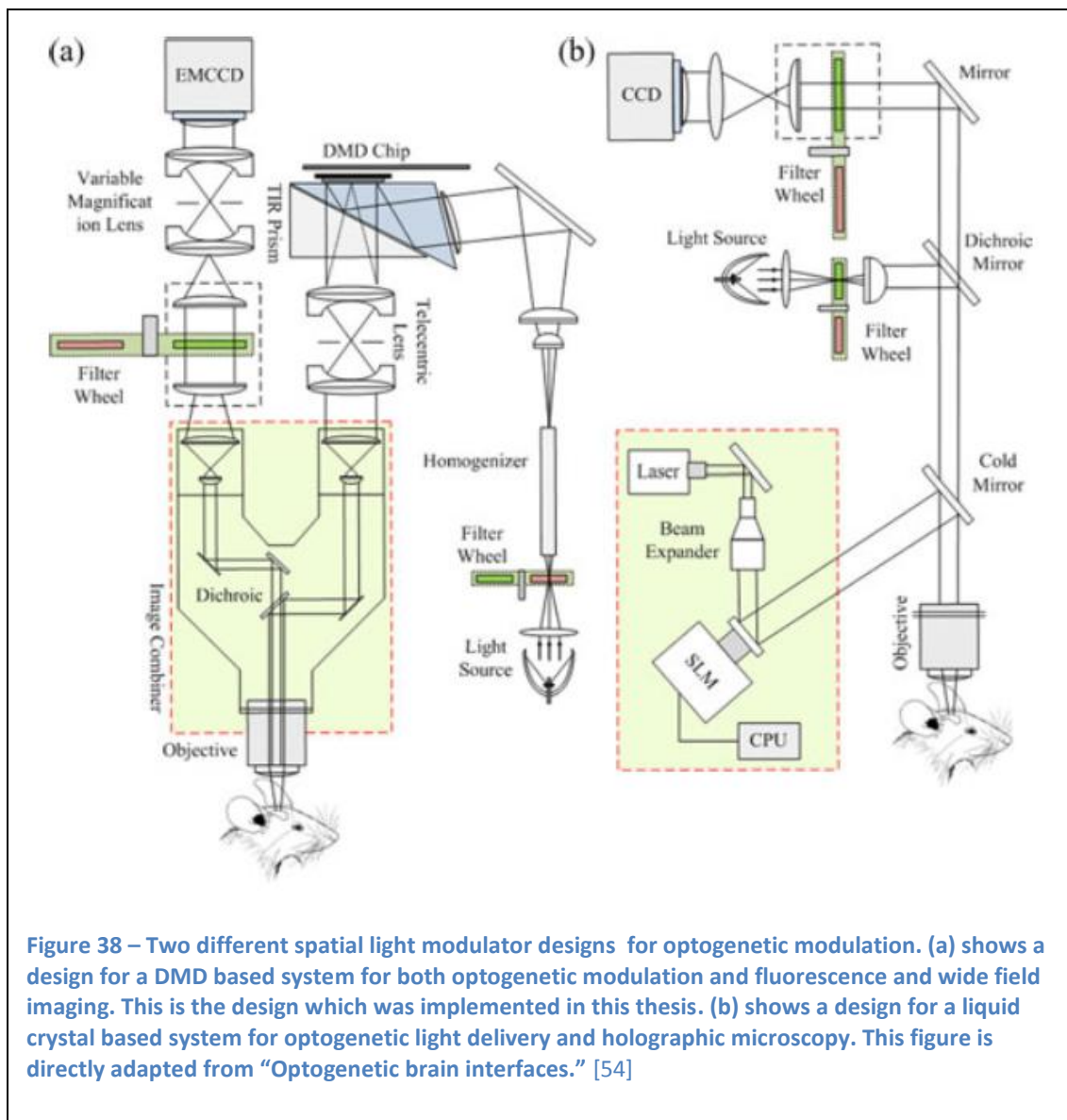
Figure 38 – Two different spatial light modulator designs for optogenetic modulation. (a) shows a design for a DMD based system for both optogenetic modulation and fluorescence and wide field imaging. This is the design which was implemented in this thesis. (b) shows a design for a liquid crystal based system for optogenetic light delivery and holographic microscopy. This figure is directly adapted from "Optogenetic brain interfaces." [54]

Developing a device which combines projection technologies with brain imaging systems allows for many more brain-machine interface device designs. Initial imaging devices used in neuroscience measured the electrical activity of the brain tissue. Over time, these technologies have evolved to more complex and accurate measuring tools. As stated earlier, patch clamp technology allows for the measurement of the membrane potential form a single neuron. An electrode can measure the local field potential of the surrounding tissue while an array of electrodes can measure multiple LFPs within tissue. Moving from electrodes to more abstract measurement techniques, fluorescent indicators fluoresce with different intensities depending upon the electric potential. As presented in this thesis, one could use blood flow or blood vessel diameter as an indicator of neural activity as well as intrinsic fluorescent molecules which are directly involved in cell metabolism such as NADH or FAD.

Combining these many types of optogenetic neuromodulation techniques with the many brain imaging systems opens possibilities for new experiments. These new experiments could help to provide insight into the workings of neural circuits, neural function, or maybe neural circuit development. Using optogenetic modulation while monitoring activity within the brain using fMRI could be of great importance for a simple fact that fiber optics are compatible with the fMRI design. With optogenetic research in its infancy, there are many opportunities to think of novel experiments which could prove to be of great importance to neuroscience and the collective understanding of how our brains function.

Chapter VII.   Concluding Remarks

The optogenetic brain-machine interface and light distribution simulation tools developed during my collaboration with the Laboratory of Optical and Computational Instrumentation (LOCI), Neural Interface Technology Research Optimization Laboratory (NITRO), and members of the Bio-Inspired Sciences and Technologies laboratory (BIST). Notably, from BIST labs, Mehdi Azimipour, Ryan Falk, and of course, my advisor and mentor, Dr. Ramin Pashaie, from LOCI and NITRO labs, Thomas Richner, Sarah Brodnik, Dr. Kevin Eliceiri, and Dr. Justin Williams. These individuals have helped address some of the important issues which face optogenetics as well as developing complex BMI systems which could someday provide robust therapeutic benefits to many people suffering from debilitating neurological diseases, disorders, and brain injuries.

These initial device designs have shown that many complex spatiotemporal closed-loop control therapies for addressing brain malfunctions are feasible. With some technological advances in imaging and SLM technology, we could possibly design systems for mobile use where a patient could carry the corrective BMI with them as they

conduct their daily tasks. Along with the potential future therapeutic benefits of this research, there are many scientific questions which could be addressed by employing a similar device to our optogenetic BMI. One possible area of scientific research which could be investigated clearly and on a timescale equivalent to that of neural activity by using optogenetics, is the interactions between neurons within complex circuits in-vitro. Another interesting area of research which has become possible more feasible by employing a optogenetic BMI device is the construction of neural circuits, in-vitro, using patterned stimulation and inhibition to develop a pre-determined desired signal processing system. This type of research would be very similar to the work being conducted at the Potter Lab of Georgia Tech [58], which utilize electrode arrays to build connections and computational networks within populations of neurons. Instead of using electrodes to build these networks in-vitro the investigator would use an optogenetic BMI device similar to the one presented in this thesis which has spatial-temporal control of the stimulation and inhibition of neurons in the field of view.

Another future application of the optogenetic BMI, given many technological advances in miniaturizing the imaging and projection devices, is a device which communicates directly to the cortex of the brain. This could include using a device to bypass the early sensors and circuits in the visual, motor, audio, or other sensory systems. There are currently devices which utilize electrodes to do restorative therapies which bypass human sensors and early brain circuits to provide artificial visual stimulation to patients who have lost their visual organs [59].

By employing the use of the Monte Carlo light distribution toolbox, one can be sure to only alter or affect the neural activity of targeted brain tissue areas for

experiments where optogenetics is employed. Although our initial Monte Carlo toolbox will only use Sprague-Dawley rats, the same or a similar device can be used to extract the optical properties of other tissues.

While optogenetics is only in the early stages of developement, the spatiotemporal optogenetic BMI and the Monte Carlo toolbox for predicting light distribution within the brain tissue address some of the concerns and technological questions which, until now, have been unanswered.

[1]   M. F. Bear, B. Connors W, and M. A. Paradiso, *Neuroscience, Exploring the Brain, 3rd Edition*. Lippincott Williams & Wilkins, 2007.

[2]   N. National Institutes of Health, "Brain Initiative," 2013.

[3]   "The Human Brain Project - Human Brain Project," 2013. [Online]. Available: https://www.humanbrainproject.eu/. [Accessed: 20-Nov-2013].

[4]   "National Human Genome Research Institute (NHGRI) - Homepage," 2013. [Online]. Available: http://www.genome.gov/. [Accessed: 20-Nov-2013].

[5]   National Institues of Health, "Nov. 2011: Human Genome Project produces many benefits," 2011. [Online]. Available: http://www.genome.gov/27549135. [Accessed: 20-Nov-2013].

[6]   "WHO | Neurological disorders affect millions globally: WHO report."

[7]   E. D. ADRIAN and Y. ZOTTERMAN, "The impulses produced by sensory nerve endings," *J. Physiol.*, pp. 151–71.

[8]   G. L. Siegel, B. W. Agranoff, R. W. Albers, and E. Al, *Basic Neurochemistry: Molecular, Cellular and Medical Aspects. 6th edition.* Philadelphia: Lippincott-Raven, 1999.

[9]   R. B. Buxton, E. C. Wong, and L. R. Frank, "Dynamics of blood flow and oxygenation changes during brain activation: the balloon model.," *Magn. Reson. Med.*, vol. 39, no. 6, pp. 855–64, Jun. 1998.

[10]   Magistretti, J. Pierre, Pellerin, Luc, Martin, and Jean-Luc, "Brain Energy Metabolism," in *Psychopharmacology - 4th Generation of Progress*, New York: Raven Press, 1995.

[11]   J. S. Perlmutter and J. W. Mink, "Deep brain stimulation.," *Annu. Rev. Neurosci.*, vol. 29, pp. 229–57, Jan. 2006.

[12]   M. S. A. Graziano, C. S. R. Taylor, and T. Moore, "Complex movements evoked by microstimulation of precentral cortex," *Neuron*, vol. 34, pp. 841–851, 2002.

[13]   E. S. Boyden, F. Zhang, E. Bamberg, G. Nagel, and K. Deisseroth, "Millisecond-timescale, genetically targeted optical control of neural activity.," *Nat. Neurosci.*, vol. 8, no. 9, pp. 1263–8, Sep. 2005.

[14]   F. Zhang, L.-P. Wang, M. Brauner, J. F. Liewald, K. Kay, N. Watzke, P. G. Wood, E. Bamberg, G. Nagel, A. Gottschalk, and K. Deisseroth, "Multimodal fast optical interrogation of neural circuitry.," *Nature*, vol. 446, no. 7136, pp. 633–9, Apr. 2007.

[15] V. Gradinaru, K. R. Thompson, F. Zhang, M. Mogri, K. Kay, M. B. Schneider, and K. Deisseroth, "Targeting and readout strategies for fast optical neural control in vitro and in vivo.," *J. Neurosci.*, vol. 27, no. 52, pp. 14231–8, Dec. 2007.

[16] J. Mattis, K. M. Tye, E. a Ferenczi, C. Ramakrishnan, D. J. O'Shea, R. Prakash, L. a Gunaydin, M. Hyun, L. E. Fenno, V. Gradinaru, O. Yizhar, and K. Deisseroth, "Principles for applying optogenetic tools derived from direct comparative analysis of microbial opsins.," *Nat. Methods*, vol. 9, no. 2, pp. 159–72, Feb. 2012.

[17] T. J. Richner, S. Thongpang, S. K. Brodnick, A. a Schendel, R. W. Falk, L. a Krugner-Higby, R. Pashaie, and J. C. Williams, "Optogenetic micro-electrocorticography for modulating and localizing cerebral cortex activity.," *J. Neural Eng.*, vol. 11, no. 1, p. 016010, Feb. 2014.

[18] K. M. Aló and J. Holsheimer, "New trends in neuromodulation for the management of neuropathic pain.," *Neurosurgery*, vol. 50, no. 4. pp. 690–703; discussion 703–4, Apr-2002.

[19] N. P. Bechtereva, a N. Bondartchuk, V. M. Smirnov, L. a Meliutcheva, and a N. Shandurina, "Method of electrostimulation of the deep brain structures in treatment of some chronic diseases.," *Confinia neurologica*, vol. 37, no. 1–3. pp. 136–40, Jan-1975.

[20] A. L. Benabid, P. Pollak, C. Gross, D. Hoffmann, A. Benazzouz, D. M. Gao, A. Laurent, M. Gentil, and J. Perret, "Acute and Long-Term Effects of Subthalamic Nucleus Stimulation in Parkinson's Disease," *Stereotact. Funct. Neurosurg.*, vol. 62, no. 1–4, pp. 76–84, 1994.

[21] a L. Benabid, P. Pollak, a Louveau, S. Henry, and J. de Rougemont, "Combined (thalamotomy and stimulation) stereotactic surgery of the VIM thalamic nucleus for bilateral Parkinson disease.," *Applied neurophysiology*, vol. 50, no. 1–6. pp. 344–6, Jan-1987.

[22] C. O. Oluigbo and A. R. Rezai, "Addressing Neurological Disorders With Neuromodulation," vol. 58, no. 7, pp. 1907–1917, 2011.

[23] M. Porta, a Brambilla, a E. Cavanna, D. Servello, M. Sassi, H. Rickards, and M. M. Robertson, "Thalamic deep brain stimulation for treatment-refractory Tourette syndrome: two-year outcome.," *Neurology*, vol. 73, no. 17, pp. 1375–80, Oct. 2009.

[24] R. J. Maciunas, B. N. Maddux, D. E. Riley, C. M. Whitney, M. R. Schoenberg, P. J. Ogrocki, J. M. Albert, and D. J. Gould, "Prospective randomized double-blind trial of bilateral thalamic deep brain stimulation in adults with Tourette syndrome.," *J. Neurosurg.*, vol. 107, no. 5, pp. 1004–14, Nov. 2007.

[25] C. H. Halpern, J. a Wolf, T. L. Bale, A. J. Stunkard, S. F. Danish, M. Grossman, J. L. Jaggi, M. S. Grady, and G. H. Baltuch, "Deep brain stimulation in the treatment of obesity.," *J. Neurosurg.*, vol. 109, no. 4, pp. 625–34, Oct. 2008.

[26] A. W. Laxton, D. F. Tang-Wai, M. P. McAndrews, D. Zumsteg, R. Wennberg, R. Keren, J. Wherrett, G. Naglie, C. Hamani, G. S. Smith, and A. M. Lozano, "A phase I trial of deep brain stimulation of memory circuits in Alzheimer's disease.," *Ann. Neurol.*, vol. 68, no. 4, pp. 521–34, Oct. 2010.

[27] C. Hamani, M. P. McAndrews, M. Cohn, M. Oh, D. Zumsteg, C. M. Shapiro, R. a Wennberg, and A. M. Lozano, "Memory enhancement induced by hypothalamic/fornix deep brain stimulation.," *Ann. Neurol.*, vol. 63, no. 1, pp. 119–23, Jan. 2008.

[28] J. Kuhn, R. Bauer, S. Pohl, D. Lenartz, W. Huff, E. H. Kim, J. Klosterkoetter, and V. Sturm, "Observations on unaided smoking cessation after deep brain stimulation of the nucleus accumbens.," *Eur. Addict. Res.*, vol. 15, no. 4, pp. 196–201, Jan. 2009.

[29] S. W. Cheung and P. S. Larson, "Tinnitus modulation by deep brain stimulation in locus of caudate neurons (area LC).," *Neuroscience*, vol. 169, no. 4, pp. 1768–78, Sep. 2010.

[30] M. Israël, H. Steiger, T. Kolivakis, L. McGregor, and A. F. Sadikot, "Deep brain stimulation in the subgenual cingulate cortex for an intractable eating disorder.," *Biol. Psychiatry*, vol. 67, no. 9, pp. e53–4, May 2010.

[31] G. E. Gibson, A. Lajtha, and G. Al Dienel, *Handbook of Neurochemistry and Molecular Neurobiology: Brain Energetics. Integration of Molecular and Cellular Processes, Volume 2*. Springer, 2007.

[32] A. Report, "DLP ^{TM} System Optics," no. July, pp. 1–26, 2010.

[33] A. Report, "DMD 101 : Introduction to Digital Micromirror Device (DMD)," no. October, pp. 1–11, 2013.

[34] Photometrics, "Evolve 512 datasheet," pp. 1–4, 2013.

[35] R. Falk, "DEVELOPMENT OF OPTOELECTRONIC PROBES FOR OPTICAL INTERROGATION OF NEURAL CIRCUITS," University of Wisconsin - Milwaukee, 2012.

[36] E. B. Bromfield, J. E. Cavazos, and J. I. Sirven, *An Introduction to Epilepsy*. West Hartford: American Epilepsy Society, 2006.

[37]   N. K. Logothetis, J. Pauls, M. Augath, T. Trinath, and a Oeltermann, "Neurophysiological investigation of the basis of the fMRI signal.," *Nature*, vol. 412, no. 6843, pp. 150–7, Jul. 2001.

[38]   I. Kahn, M. Desai, U. Knoblich, J. Bernstein, M. Henninger, A. M. Graybiel, E. S. Boyden, R. L. Buckner, and C. I. Moore, "Characterization of the functional MRI response temporal linearity via optical control of neocortical pyramidal neurons.," *J. Neurosci.*, vol. 31, no. 42, pp. 15086–91, Oct. 2011.

[39]   P. J. Drew, A. Y. Shih, J. D. Driscoll, P. M. Knutsen, P. Blinder, D. Davalos, K. Akassoglou, P. S. Tsai, and D. Kleinfeld, "Chronic optical access through a polished and reinforced thinned skull," vol. 7, no. 12, pp. 5–10, 2010.

[40]   T. J. Richner, R. Baumgartner, S. K. Brodnick, M. Azimipour, L. A. Krugner-higby, and K. W. Eliceiri, "Patterned optogenetic modulation of neurovascular and metabolic signals," *J. Cereb. Blood Flow Metab.*, no. 20610, pp. 1–8, 2014.

[41]   M. Guizar-Sicairos, S. T. Thurman, and J. R. Fienup, "Efficient subpixel image registration algorithms.," *Opt. Lett.*, vol. 33, no. 2, pp. 156–8, Jan. 2008.

[42]   J. H. Lee, R. Durand, V. Gradinaru, F. Zhang, I. Goshen, D.-S. Kim, L. E. Fenno, C. Ramakrishnan, and K. Deisseroth, "Global and local fMRI signals driven by neurons defined optogenetically by type and wiring.," *Nature*, vol. 465, no. 7299, pp. 788–92, Jun. 2010.

[43]   M. Desai, I. Kahn, U. Knoblich, J. Bernstein, H. Atallah, a Yang, N. Kopell, R. L. Buckner, a M. Graybiel, C. I. Moore, and E. S. Boyden, "Mapping brain networks in awake mice using combined optical neural control and fMRI.," *J. Neurophysiol.*, vol. 105, no. 3, pp. 1393–405, Mar. 2011.

[44]   E. Lothman, J. Lamanna, G. Cordingley, M. Rosenthal, and G. Somjen, "Responses of electrical potential, potassium levels, and oxidative metabolic activity of the cerebral neocortex of cats.," *Brain research*, vol. 88, no. 1. pp. 15–36, 25-Apr-1975.

[45]   T. Vo-Dinh, *Biomedical Photonics Handbook, Ed. 1*. 2003.

[46]   S. A. Prahl, M. J. C. Van Gemert, and A. J. Welch, "Determining the optical properties of turbid media," vol. 32, no. 4, pp. 559–568, 1993.

[47]   J. W. Pickering, S. a Prahl, N. van Wieringen, J. F. Beek, H. J. Sterenborg, and M. J. van Gemert, "Double-integrating-sphere system for measuring the optical properties of tissue.," *Appl. Opt.*, vol. 32, no. 4, pp. 399–410, Feb. 1993.

[48] "A computer simulation of the distribution of light within a complex tissue SOFTWARE." [Online]. Available: http://omlc.org/software/mc/mcxyz/index.html. [Accessed: 13-Aug-2014].

[49] L. Wang, S. L. Jacques, and L. Zheng, "MCML--Monte Carlo modeling of light transport in multi-layered tissues.," *Computer methods and programs in biomedicine*, vol. 47, no. 2. pp. 131–46, Jul-1995.

[50] D. F. Levinson, "The genetics of depression: a review.," *Biol. Psychiatry*, vol. 60, no. 2, pp. 84–92, Jul. 2006.

[51] J. Talan, *Deep Brain Stimulation: A New Treatment Shows Promise in the Most Difficult Cases*, 1st ed. New York: Dana Press, 2009.

[52] K. L. Chou, S. Grube, and P. G. Patil, *Deep Brain Stimulation: A New Life for People with Parkinson's, Dystonia, and Essential Tremor*, 1st ed. New York: Demos medical Printing, 2012.

[53] R. a Normann, E. M. Maynard, P. J. Rousche, and D. J. Warren, "A neural interface for a cortical vision prosthesis.," *Vision Res.*, vol. 39, no. 15, pp. 2577–87, Jul. 1999.

[54] R. Pashaie, P. Anikeeva, J. H. Lee, R. Prakash, O. Yizhar, M. Prigge, D. Chander, T. J. Richner, and J. Williams, "Optogenetic brain interfaces.," *IEEE Rev. Biomed. Eng.*, vol. 7, pp. 3–30, Jan. 2014.

[55] R. Pashaie and R. Falk, "Single optical fiber probe for fluorescence detection and optogenetic stimulation.," *IEEE Trans. Biomed. Eng.*, vol. 60, no. 2, pp. 268–80, Feb. 2013.

[56] A. N. Zorzos, J. Scholvin, E. S. Boyden, and C. G. Fonstad, "Three-dimensional multiwaveguide probe array for light delivery to distributed brain circuits.," *Opt. Lett.*, vol. 37, no. 23, pp. 4841–3, Dec. 2012.

[57] A. N. Zorzos, E. S. Boyden, and C. G. Fonstad, "Multiwaveguide implantable probe for light delivery to sets of distributed brain targets.," *Opt. Lett.*, vol. 35, no. 24, pp. 4133–5, Dec. 2010.

[58] NeuroLab, "Potter Lab Research," 2014. [Online]. Available: https://neurolab.gatech.edu/labs/potter/research. [Accessed: 08-Apr-2014].

[59] W. H. Dobelle, "Artificial vision for the blind by connecting a television camera to the visual cortex.," *ASAIO J.*, vol. 46, no. 1, pp. 3–9, 2000.

[60] M. A. A. Khalid, "Membrane Electrochemistry: Electrochemical Processes in Bilayer Lipid Membrane," in *Electrochemistry*, pp. 71–92.

[61] W. Gerstner and W. Kistler, *Spiking Neuron Models: Single Neurons, Populations, Plasticity*. Cambridge University Press, 2002, pp. 1–480.

[62] J. H. P. D. Byrne, "Introduction to Neurons and Neuronal Networks." [Online]. Available: http://neuroscience.uth.tmc.edu/s1/introduction.html.

[63] F. Zhang, A. M. Aravanis, and A. Adamantidis, "Circuit-breakers: optical technologies for probing neural signals and systems.," vol. 8, no. August, pp. 577–581, 2007.

[64] T. Richner, R. Baumgartner, S. Brodnick, M. Azimipour, K. Eliceiri, and J. Williams, "Closed-Loop Optogenetic Brain Interface," pp. 1–12.

[65] M. Azimipour, R. Baumgartner, Y. Liu, S. L. Jacques, K. Eliceiri, and R. Pashaie, "Extraction of optical properties and prediction of light distribution in rat brain tissue.," *J. Biomed. Opt.*, vol. 19, no. 7, p. 75001, Jul. 2014.